EUROPEAN ORGANIZATION FOR NUCLEAR RESEARCH (CERN)

CERN-EP-2023-110
2024/02/07

CMS-HIG-22-009

Measurement of the Higgs boson production via vector boson fusion and its decay into bottom quarks in proton-proton collisions at $\sqrt{s} = 13\,\text{TeV}$

The CMS Collaboration*

arXiv:2308.01253v2 [hep-ex] 6 Feb 2024

Abstract

A measurement of the Higgs boson (H) production via vector boson fusion (VBF) and its decay into a bottom quark-antiquark pair ($\mathrm{b\bar{b}}$) is presented using proton-proton collision data recorded by the CMS experiment at $\sqrt{s} = 13\,\text{TeV}$ and corresponding to an integrated luminosity of $90.8\,\text{fb}^{-1}$. Treating the gluon-gluon fusion process as a background and constraining its rate to the value expected in the standard model (SM) within uncertainties, the signal strength of the VBF process, defined as the ratio of the observed signal rate to that predicted by the SM, is measured to be $\mu^{\mathrm{qqH}}_{\mathrm{Hb\bar{b}}} = 1.01^{+0.55}_{-0.46}$. The VBF signal is observed with a significance of 2.4 standard deviations relative to the background prediction, while the expected significance is 2.7 standard deviations. Considering inclusive Higgs boson production and decay into bottom quarks, the signal strength is measured to be $\mu^{\text{incl.}}_{\mathrm{Hb\bar{b}}} = 0.99^{+0.48}_{-0.41}$, corresponding to an observed (expected) significance of 2.6 (2.9) standard deviations.

Published in the Journal of High Energy Physics as doi:10.1007/JHEP01(2024)173.

© 2024 CERN for the benefit of the CMS Collaboration. CC-BY-4.0 license

*See Appendix A for the list of collaboration members

1 Introduction

Following the discovery of a scalar boson with a mass near 125 GeV by the ATLAS and CMS Collaborations [1–3] at the CERN LHC, extensive studies of the properties of this particle have been pursued. A multitude of measurements performed thus far in various production and decay modes support the hypothesis that the discovered particle is the Higgs boson (H) described by the standard model (SM) that arises as a consequence of the Brout–Englert–Higgs mechanism of the electroweak (EW) symmetry breaking [4–9].

The SM Higgs boson with mass of 125 GeV decays most frequently into a bottom quark-antiquark ($\mathrm{b\bar{b}}$) pair with a branching fraction of about 58% [10, 11]. However, it is challenging to explore this decay mode experimentally. In the dominant gluon-gluon fusion (ggH) production mode, the $\mathrm{H} \to \mathrm{b\bar{b}}$ signal is overwhelmed by a background consisting of $\mathrm{b\bar{b}}$ pairs produced through the strong interaction, referred to as quantum chromodynamics (QCD) multijet events. At the LHC, a moderate sensitivity to the $\mathrm{H} \to \mathrm{b\bar{b}}$ decay in the ggH process can be achieved by exploiting Lorentz-boosted production of the Higgs boson [12, 13]. The most promising production mechanism to study the $\mathrm{H} \to \mathrm{b\bar{b}}$ decay is the Higgs boson production in association with a leptonically decaying W or Z boson (VH). Although the VH production cross section is more than an order of magnitude smaller than that of ggH, leptonic decays of W and Z bosons provide a handle to reduce backgrounds, thereby making the $\mathrm{H} \to \mathrm{b\bar{b}}$ decay accessible for detection. The VH production mode has contributed with the largest sensitivity to the observation of the $\mathrm{H} \to \mathrm{b\bar{b}}$ decay by the CMS and ATLAS Collaborations. The ATLAS Collaboration has measured the $\mathrm{H} \to \mathrm{b\bar{b}}$ signal yield relative to the SM prediction to be $\mu^{\mathrm{incl.}}_{\mathrm{Hb\bar{b}}} = 1.02 \pm 0.12\,(\mathrm{stat}) \pm 0.14\,(\mathrm{syst})$, corresponding to a significance of 6.7 standard deviations (σ) [14] using 139 fb^{-1} of pp collisions data collected at the center-of-mass energy ($\sqrt{s}$) of 13 TeV. The measurement by CMS is $\mu^{\mathrm{incl.}}_{\mathrm{Hb\bar{b}}} = 1.04 \pm 0.14\,(\mathrm{stat}) \pm 0.14\,(\mathrm{syst})$ and corresponds to a significance of $5.6\,\sigma$ [15] by combining VH along with other production modes using the data collected at $\sqrt{s} = 7$, 8 and 13 TeV in 2011–2017. Both the ATLAS and CMS Collaborations have also pursued studies of the Higgs boson production in association with top quark-antiquark pairs, followed by the $\mathrm{H} \to \mathrm{b\bar{b}}$ decay. The rate of this process relative to the SM prediction has been measured to be $0.35^{+0.36}_{-0.34}$ by the ATLAS Collaboration [16] and 0.33 ± 0.26 by the CMS Collaboration [17].

This paper considers the vector boson fusion (VBF) production mechanism for the detection of the $\mathrm{H} \to \mathrm{b\bar{b}}$ signal. The VBF production of the Higgs boson has the second-largest cross section at the LHC and attracts particular attention because it involves large momentum transfer and provides a sensitive probe of momentum-dependent anomalous couplings [18].

The VBF production followed by the $\mathrm{H} \to \mathrm{b\bar{b}}$ decay, $\mathrm{qqH} \to \mathrm{qqb\bar{b}}$, gives rise to a four-jet final state as depicted in Fig. 1. Two of the jets, from the $\mathrm{H} \to \mathrm{b\bar{b}}$ decay, typically lie in the central region of the detector. The other two jets, from the light quarks, are produced mainly in the forward and backward directions relative to the beam line and, consequently, have a large rapidity separation between them, as well as high dijet invariant mass. We refer to the latter as VBF jets. As the interaction proceeds via the exchange of colorless particles (V = W or Z), the color connection between the outgoing light-flavor quarks is suppressed, leading to a relatively small amount of hadronic activity in the rapidity interval between the VBF jets and b-tagged jets originating from the Higgs boson decay. These distinct features allow for the suppression of the large QCD multijet background and the identification of the signal process.

The previous measurement of the $\mathrm{qqH} \to \mathrm{qqb\bar{b}}$ process by the CMS Collaboration is based on a data set of proton-proton (pp) collisions at $\sqrt{s} = 8$ TeV, corresponding to an integrated

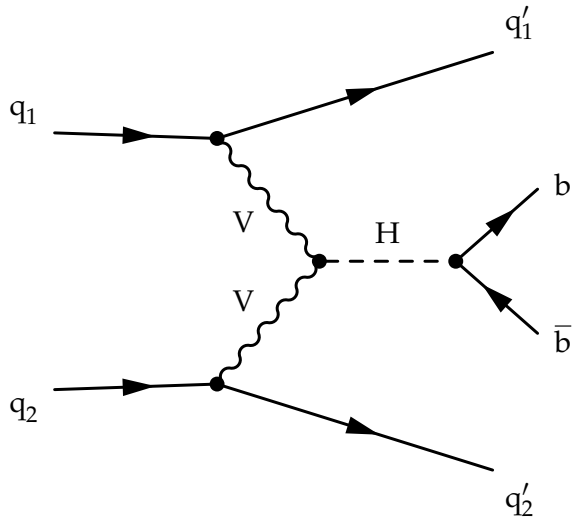

Figure 1: Representative Feynman diagram of the leading order (LO) VBF production of a Higgs boson, followed by its decay to a pair of b quarks.

luminosity of about $20\,\text{fb}^{-1}$ [19]. The signal strength was observed to be $\mu^{\text{qqH}}_{\text{Hb}\bar{\text{b}}} = 2.8^{+1.6}_{-1.4}$ with a significance of $2.2\,\sigma$, while the expected significance was $0.8\,\sigma$. The ATLAS Collaboration recently reported a measurement of the $\text{qqH} \to \text{qqb}\bar{\text{b}}$ process using data collected in pp collisions at $\sqrt{s} = 13\,\text{TeV}$, corresponding to an integrated luminosity of $127\,\text{fb}^{-1}$ [20] and the signal strength was measured to be $\mu^{\text{qqH}}_{\text{Hb}\bar{\text{b}}} = 0.95^{+0.38}_{-0.36}$, corresponding to an observed (expected) significance of 2.6 (2.8) σ.

In this paper, we present a measurement of the $\text{qqH} \to \text{qqb}\bar{\text{b}}$ process using data collected by CMS at $\sqrt{s} = 13\,\text{TeV}$. The paper is organized as follows. In Section 2 the main features of the CMS detector are outlined. Section 3 describes the reconstruction of physics objects relevant for this analysis. Data sets and simulated samples used in the study are presented in Section 4, and Section 5 describes employed triggers. Details of the offline analysis, including the event selection and categorization, the improvement of the jet transverse momentum (p_{T}) resolution by regression techniques, background estimation methods, and signal extraction procedure are discussed in Section 6. Section 7 details the main systematic uncertainties affecting the analysis. The final results are discussed in Section 8 and a brief summary is given in Section 9. The tabulated results are provided in a HEPData record [21].

2 The CMS detector

The central feature of the CMS apparatus is a superconducting solenoid of 6 m internal diameter, providing a magnetic field of 3.8 T along the beam direction. Within the solenoid volume are a silicon pixel and strip tracker, a lead tungstate crystal electromagnetic calorimeter (ECAL), and a brass and scintillator hadron calorimeter (HCAL), each composed of a barrel and two endcap sections. The ECAL consists of 75 848 lead tungstate crystals, which provide coverage in pseudorapidity $|\eta| < 1.48$ in the barrel (EB) region and $1.48 < |\eta| < 3.00$ in the two endcap (EE) regions. Preshower detectors consisting of two planes of silicon sensors interleaved with a total of 3 radiation lengths of lead are located in front of each endcap detector. Forward calorimeters extend the η coverage provided by the barrel and endcap detectors. Muons are detected in gas-ionization chambers embedded in the steel flux-return yoke outside the solenoid.

Events of interest are selected using a two-tiered trigger system [22]. The first level (L1), composed of custom hardware processors, uses information from the calorimeters and the muon subdetectors to select events at a rate of around 100 kHz within a fixed time interval of less than 4 μs. The second level, known as the high-level trigger (HLT), consists of a farm of processors running a version of the full event reconstruction software optimized for fast processing, and reduces the event rate to around 1 kHz before data storage [23].

A more detailed description of the CMS detector, together with a definition of the coordinate system used and the relevant kinematic variables, can be found in Ref. [24].

3 Event reconstruction

The reconstruction of the physics objects at CMS is based on the particle-flow (PF) algorithm [25], which aims to reconstruct and identify each individual particle (PF candidate) in an event, with an optimized combination of information from the various elements of the CMS detector.

For each event, hadronic jets are clustered from these reconstructed particles using the infrared- and collinear-safe anti-k_{T} algorithm [26, 27] with a distance parameter of 0.4. The jet momentum is determined as the vectorial sum of all particle momenta in the jet, which is typically within 5 to 10% of the true momentum over the entire range of kinematically allowed p_{T} and the detector acceptance. Additional pp interactions within the same or nearby bunch crossings (pileup) increase the track multiplicity and calorimetric energy depositions which, potentially affects the jet momentum. To mitigate this effect, charged particles identified to be originating from pileup vertices are discarded and an offset correction is applied to account for the remaining contributions. Jet energy corrections are derived from simulation to match the measured response of the reconstructed jets to that of particle level-jets on average. In-situ measurements of the momentum balance in dijet, photon+jets, Z+jets and multijet events are used to account for any residual differences in the jet energy scale between data and simulation [28]. The jet energy resolution amounts typically to 15–20% at 30 GeV, 10% at 100 GeV, and 5% at 1 TeV [28]. Additional selection criteria are applied to remove jets potentially dominated by anomalous contributions from various subdetector components or reconstruction failures.

At the HLT, identification of the jets resulting from the hadronization of b-quarks is performed with the combined secondary vertex algorithm (CSV) [29, 30] and with its improved version using deep machine learning technique (DEEPCSV) [30]. These algorithms combine the information from track impact parameters and secondary vertices identified within a given jet, and provide a continuous discriminator output. A jet with a CSV or DEEPCSV discriminant value above a certain threshold is considered to be b-tagged. The efficiency for tagging b jets and the rate at which light-flavor, gluon, and charm jets are misidentified as b jets depend on the chosen threshold, as well as on the jet p_{T} and η. The thresholds are chosen to ensure an online selection of b jets with an efficiency of 60–70%, corresponding to a misidentification rate of 2–3%. Identification of b jets in the offline analysis is performed with the DEEPJET tagger [31, 32], which combines features of the individual jet constituents, properties of the reconstructed secondary vertices, and the global jet variables into a multiclass deep neural network (DNN) targeting three separate classes for the b jets: i) jet with one B hadron, ii) jet with two or more B hadrons, and iii) jet with semileptonic decays of B hadrons. The sum of three b tag class DNN outputs quantifies the consistency of a jet with the b jet hypothesis. A jet is considered to be b-tagged in the offline selection, if this DNN output, referred to as the b tag score, exceeds a certain threshold. These thresholds are chosen such that the b jet selection efficiency is 70–80% depending on data-taking periods, while the probability of light and gluon jets being misidentified as b jets is about 1% and the probability of charm jets being misidentified as b jets is about 10%.

To minimize the discrepancy in the b tagging performance between data and simulation both at the HLT and in the offline analysis, separate jet flavor dependent calibration factors are applied to each jet in simulated events as a function of jet p_T, η, and the b tag discriminator score. These corrections have been derived using control samples of the semileptonic $t\bar{t}$ decays, Z+jets events, and the inclusive sample of QCD multijet events [30]. Determination of corrections at the HLT is facilitated by the control and prescaled single- and multi-jet triggers.

4 Data set and simulated samples

This analysis uses data collected by the CMS experiment in pp collisions at $\sqrt{s} = 13\,\text{TeV}$ corresponding to an integrated luminosity of $90.8\,\text{fb}^{-1}$. The total analyzed data volume comprises two sets recorded under different experimental conditions. The first set was collected in 2016 and corresponds to an integrated luminosity of $36.3\,\text{fb}^{-1}$. The second set was collected in 2018, when the LHC delivered pp collisions at higher instantaneous luminosity compared to 2016, and corresponds to an integrated luminosity of $54.5\,\text{fb}^{-1}$. No trigger path suitable for this analysis was available during the data-taking periods in 2017.

The analysis relies on simulated Monte Carlo (MC) samples for the estimation of the signal acceptance and efficiency and determination of the trigger efficiency. Additionally, the contributions from various subdominant background processes are determined from simulation.

The $qqH \to qqb\bar{b}$ signal is generated using POWHEG 2.0 [33–35] at next-to-leading order (NLO) precision in the QCD coupling constant α_S [36]. A dipole parton shower model [37] incorporated in PYTHIA 8.212 [38] is used for emulating of the initial-final state color flow that takes into account the color connection between the incoming and the outgoing partons. An alternative $qqH \to qqb\bar{b}$ sample is also prepared using the POWHEG matrix element generator interfaced with HERWIG 7 v-7.1[39] for fragmentation and hadronization. This sample is used only to assess the systematic uncertainty related to the choice of the showering and hadronization model. The ggH production of the Higgs boson with at least two accompanying jets has a nonnegligible contribution to the kinematic phase space considered in this analysis. The ggH process is generated using the MiNLO event generator at next-to-NLO (NNLO) [40, 41] precision in α_S [42], including finite top quark mass effects. An NLO process that may include loops needs to be hadronized with a parton shower model beyond LO. As a result, jet matching must take into account additional hard radiative jets. This is implemented, for this analysis, by employing the FxFx scheme [43]. Contributions from the weak gauge boson associated (VH) and top-quark-pair associated ($t\bar{t}H$) production of the Higgs boson are found to be negligible.

The dominant continuum background for this analysis is QCD multijet production. To assess properties of these events and validate the analysis strategy, QCD multijet events are generated with MADGRAPH5_aMC@NLO [44] at leading order (LO) precision in α_S. The matrix element is matched to the parton showers generated by PYTHIA using the MLM prescription [45]. Generated samples of QCD multijet production are also used to derive corrections applied to simulated samples to account for differences in the trigger efficiency between data and simulation.

The dominant resonant background is the inclusive production of Z bosons (Z+jets). About 70% of the time, Z bosons decay via a quark-antiquark pair of the same flavor, including a 15% branching fraction into a pair of bottom quarks. Hence, the main component of the resonant background in the event sample corresponds to the $Z \to b\bar{b}$ decay mode, although there are contributions from charm and light-flavor quark jets being misidentified as b jets. There are two different mechanisms of Z+jets production: via quark-antiquark annihilation ($q\bar{q} \to Z$) and fusion of W bosons ($WW \to Z$). Though the latter has a much lower rate, the event topology is

the same as for the signal. W bosons can be produced in association with jets in similar ways. The inclusive W production is generated using MADGRAPH5_aMC@NLO at LO precision in α_S. The same generator is used to produce mutually exclusive $q\bar{q} \to Z$ and $WW \to Z$ samples. The $q\bar{q} \to Z$ process is simulated considering Feynman diagrams involving direct electroweak coupling of the Z boson to quark-antiquark pairs. In the generation of the $WW \to Z$ process, only the Feynman diagrams that contain the WWZ triple gauge boson coupling are considered in the computation of the matrix element. As in the case of the $qqH \to qqb\bar{b}$ signal, the $WW \to Z$ process is simulated using a dipole parton shower model implemented in PYTHIA.

For the Z+jets samples, correction factors have been applied to match the generator-level p_T distributions with analytic predictions available with the highest order accuracy in the perturbative expansion [46]. Two individual correction factors are applied to the $q\bar{q} \to Z$ process for each p_T bin; first to emulate the spectrum predicted by perturbative QCD with NNLO accuracy and then further reweighting is done to incorporate the higher-order EW effects. For the $WW \to Z$ mechanism, only higher-order EW correction factors are applied.

Other important background contributions in the signal region arise from inclusive single top quark ($t/\bar{t}$+X) and top quark pair ($t\bar{t}$+X) production. These are modeled by POWHEG [47, 48] at the NLO QCD precision. For the $t\bar{t}$ process, all possible combinations of the decay modes of the two W bosons from the top quark and antiquark decays are considered leading to hadronic, leptonic, and semileptonic final states.

All the simulated samples except the HERWIG signal sample are interfaced with PYTHIA 8.212 for parton showering and fragmentation with the standard p_T-ordered parton shower scheme. The underlying event is modeled with PYTHIA, using the CP5 tune [49] for both of the years. The parton distribution functions (PDFs) are taken from the sets of NNPDF3.0 [50] and NNPDF3.1 [51] for the 2016 and 2018 samples respectively. The response of the CMS detector is modeled using the GEANT4 [52] package. The event reconstruction is performed with the same algorithms as are used for the data. Additional pileup interactions in each bunch crossing are generated with PYTHIA and added to the simulated samples following a Poisson distribution with the mean value determined in the data. The simulated events are weighted such that the pileup distribution in the simulation matches the one observed in the data.

5 Triggers

Events are selected with dedicated L1 and HLT selections optimized separately for 2016 and 2018. At the L1 stage, events are required to have at least three jets with p_T above certain thresholds that were optimized according to the instantaneous luminosity. The p_T thresholds of 90, 76, and 64 GeV (100, 80, and 70 GeV) were imposed for 2016 (2018). The presence of a fourth jet is not required at the L1 stage.

An event is accepted by the HLT if it contains at least four jets reconstructed online with the PF algorithm. Jets are required to have p_T greater than 92, 76, 64, and 15 (105, 88, 76, and 15) GeV in 2016 (2018). Two complementary online requirements (HLT paths), as explained below, are also implemented to select events in each of the two sets. In the following, we refer to these HLT paths as `HLT_Tight` and `HLT_Loose`.

The `HLT_Tight` path selects events with at least one b-tagged jet among six leading jets according to p_T. The b tagging is performed with the CSV (DEEPCSV) algorithm in 2016 (2018). The working point chosen for the online b tagging in the `HLT_Tight` path corresponds to b jet efficiency of roughly 60 to 70% and a misidentification rate for light-flavor quark and gluon

jets of 3 to 4%. In addition to the b-tagging selection there is also a VBF-selection implemented at the HLT path, which considers only four p_T leading jets. Among these four jets, the one with the highest CSV (DEEPCSV) discriminant is considered to be a jet from the Higgs boson decay, and out of the three remaining jets, a jet pair with the largest $\Delta\eta_{jj}$ is chosen as the pair of VBF-tagged jets. The last remaining jet is considered to be the other jet from the decay of the Higgs boson. The `HLT_Tight` path imposes very stringent conditions on the VBF-tagged jets: they must be separated in pseudorapidity by $\Delta\eta_{jj} > 4.1$ (3.5) and have invariant mass $m_{jj} > 500$ (460) GeV in 2016 (2018). For the other two jets, which are assigned to the $H \to b\bar{b}$ decay, the separation in azimuthal angle is required to be $\Delta\phi_{b\bar{b}} < 1.6$ (1.9) for 2016 (2018).

In contrast to the `HLT_Tight` path, the `HLT_Loose` path selects events with at least two b-tagged jets but imposes comparatively lenient requirements on the VBF-tagged jets: $m_{jj} > 240$ (200) GeV and $\Delta\eta_{jj} > 2.3$ (1.5) for 2016 (2018); while $\Delta\phi_{b\bar{b}} < 2.1$ (2.8) in 2016 (2018) is required for b jets. Requirements imposed by the `HLT_Tight` and `HLT_Loose` paths in the 2016 and 2018 data-taking periods are summarized in Table 1.

The efficiency of the trigger selection is measured with the tag-and-probe method [53] using events selected with control triggers. Trigger scale factors, representing the ratio of the trigger efficiency in data to that in simulated events, are measured as a function of jet p_T and $|\eta|$ for each leg of the four-jet requirement using control and prescaled single-jet triggers. For the online b tagging, the scale factors are also derived as a function of the DEEPJET discriminants of the offline tagged jets employing auxiliary and prescaled four-jet triggers. The applied corrections range from 2 to 7% for each leg of the four-jet requirement and from 3 to 10% per jet for the online b tag requirement.

The absolute trigger efficiencies, computed for the inclusive simulated signal samples, are 3.1 (2.3) and 3.5 (2.5)% in 2016 (2018), for the `HLT_Tight` and `HLT_Loose` paths, respectively. The inefficiencies of the trigger paths are mainly driven by the relatively high p_T thresholds imposed on the three leading jets.

6 Analysis procedures

Events recorded online by the HLT paths described in Section 5, are reconstructed with improved information related to the detector conditions and calibrations.

6.1 Event selection

An event is discarded if it contains any isolated muon or electron identified through selection criteria that correspond to a selection efficiency of 95% and a misidentification rate of 1–2%. This requirement suppresses contributions from $t\bar{t}$ and $t/\bar{t}$ events with leptonic decays of the W bosons. The event is selected if it contains four jets with p_T greater than 95, 80, 65, and 30 GeV (110, 90, 80, and 30 GeV) in 2016 (2018). Reconstructed physics objects are matched to the corresponding trigger objects. At least two jets are required to be b tagged with the DEEPJET algorithm as described in Section 3. Out of the four p_T-leading jets, the two jets with the highest DEEPJET b tag scores are used to reconstruct the $H \to b\bar{b}$ decay candidate. After the Higgs boson candidate is selected, the two remaining jets are considered as VBF-tagged jet candidates. The jet with $p_T < 50$ GeV must also pass an identification criterion designed to reduce the number of selected jets originating from pileup interactions [54].

Depending on the data-taking periods and the trigger they pass, events are split into four nonoverlapping samples that are analyzed independently. Events from 2016 (2018) that pass

the HLT_Tight path are assigned to the Tight 2016 (Tight 2018) sample; events failing the HLT_Tight path but pass the HLT_Loose path comprise the Loose 2016 (Loose 2018) sample. The selection criteria applied to the VBF- and b-tagged jets in each sample are:

- Tight 2016: $\Delta\phi_{b\bar{b}} < 1.6$, $\Delta\eta_{jj} > 4.2$, $m_{jj} > 500\,\text{GeV}$;
- Loose 2016: $\Delta\phi_{b\bar{b}} < 2.1$, $\Delta\eta_{jj} > 2.5$, $m_{jj} > 250\,\text{GeV}$;
- Tight 2018: $\Delta\phi_{b\bar{b}} < 1.6$, $\Delta\eta_{jj} > 3.8$, $m_{jj} > 500\,\text{GeV}$; and
- Loose 2018: $\Delta\phi_{b\bar{b}} < 2.1$, $\Delta\eta_{jj} > 2.5$, $m_{jj} > 250\,\text{GeV}$.

The lower section of Table 1 outlines the selection criteria used in the offline analysis.

Table 1: The HLT and offline selection requirements in the four analyzed samples.

Level	Requirements	2016 (36.3 fb^{-1})		2018 (54.5 fb^{-1})	
		Tight	Loose	Tight	Loose
HLT	p_T thresholds	92, 76, 64, 15 GeV		105, 88, 76, 15 GeV	
	Number of b tags	$\geq$1	$\geq$2	$\geq$1	$\geq$2
	$\Delta\phi_{b\bar{b}}$	$<$1.6	$<$2.1	$<$1.9	$<$2.8
	$\Delta\eta_{jj}$	$>$4.1	$>$2.3	$>$3.5	$>$1.5
	m_{jj}	$>$ 500 GeV	$>$240 GeV	$>$460 GeV	$>$200 GeV
Offline	p_T thresholds	95, 80, 65, 30 GeV		110, 90, 80, 30 GeV	
	Jet $\lvert\eta\rvert < 4.7$	✓	✓	✓	✓
	Lepton veto	✓	✓	✓	✓
	Number of b tags ≥ 2	✓	✓	✓	✓
	b jet $\lvert\eta\rvert < 2.4$	✓	✓	✓	✓
	$\Delta\phi_{b\bar{b}}$	$<$1.6	$<$2.1	$<$1.6	$<$2.1
	$\Delta\eta_{jj}$	$>$4.2	$>$2.5	$>$3.8	$>$2.5
	m_{jj}	$>$500 GeV	$>$250 GeV	$>$500 GeV	$>$250 GeV

6.2 Regression of b jet energy

The energy of a b-tagged jet is likely to be underestimated often because of the unmeasured neutrino produced in the semileptonic decay of a b hadron. This is partially remedied by the energy regression of a b jet [55] that improves the mass resolution of the Higgs boson candidate constructed from the two b-tagged jets. The regression is based on a DNN trained on simulated b jets from $t\bar{t}$ events. The algorithm's input features include properties of the secondary vertices and tracks associated with the jet, jet constituents, soft muons and electrons from the semileptonic decays of b hadrons, as well as additional variables related to the jet energy. After the application of the b jet energy regression, the jet energy scale and resolution of b jets are corrected in simulated events to match the jet energy scale and resolution observed in data. Corrections are devised using events where a b-tagged jet recoils against a Z boson that decays into leptons. The Z boson p_T is reconstructed with high precision due to the excellent resolution of the lepton momentum. As the p_T of the Z boson is balanced with the jet p_T, the ratio of the momentum of the reconstructed jet to the Z boson momentum is used to measure the jet energy scale and resolution in the data and simulated samples and derive corresponding corrections to the energy scale and resolution of b jets in the simulated events. The correction factors constitute about 0.5–2% (1–4%) of the jet p_T for the resolution (scale) of the regressed jets. As an illustration, Fig. 2 shows the effect of b jet energy regression on the invariant mass $m_{b\bar{b}}$ of the reconstructed b jet pair in simulated $qqH \to qqb\bar{b}$ signal events for the Tight

2016 and Loose 2016 samples. Distributions of $m_{b\bar{b}}$ are obtained after applying dedicated corrections to the energy scale and resolution of b jets in simulated events. The b jet energy regression improves the $m_{b\bar{b}}$ resolution and the central value by approximately 10 to 15%.

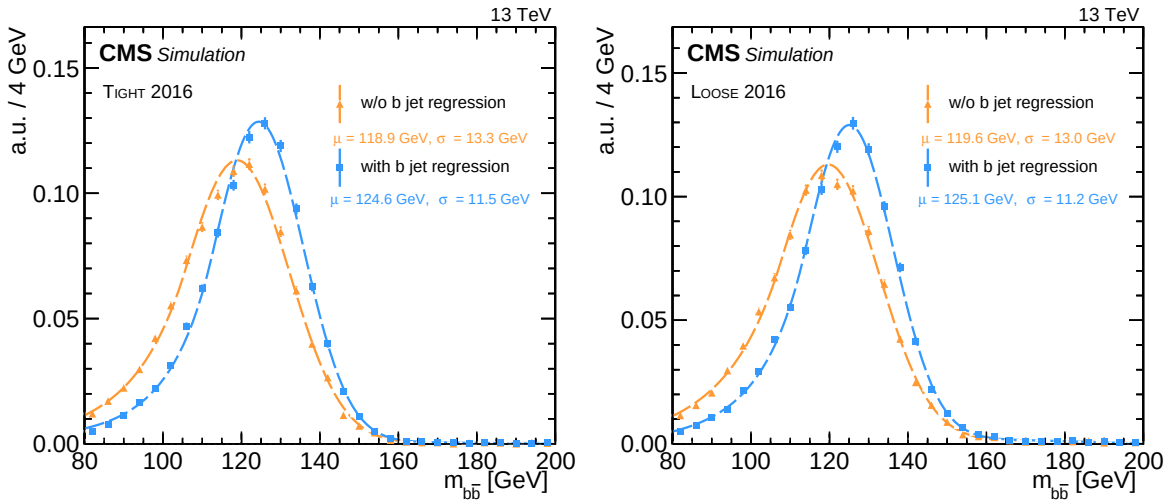

Figure 2: The invariant mass $m_{b\bar{b}}$ of the b jet pair in simulated $qqH \to qqb\bar{b}$ events before (orange dashed line) and after (blue dashed line) the application of the b jet energy regression in the Tight 2016 (left) and Loose 2016 (right) samples. A one-sided Crystal Ball function [56] is used to fit the distributions, where μ and σ are the peak position and half width of the core part of the CB function, respectively.

6.3 Event categorization

To discriminate the signal from the major background sources, a multivariate analysis (MVA) technique is applied; the key properties of the $qqH \to qqb\bar{b}$ signal are combined in a boosted decision tree (BDT) algorithm implemented with the TMVA package [57]. The BDT response is then used to separate the signal from the background processes. Two different MVA strategies are applied in the Tight and Loose samples.

The Tight 2016 and Tight 2018 samples are characterized by lower background yields and higher signal-to-background ratios. In particular, the contributions from the resonant $Z \to b\bar{b}$ background and ggH production are significantly suppressed by more stringent requirements imposed on the VBF-tagged jets. The largest background in these event classes originates from the QCD multijet production. Two separate binary classifiers are trained to discriminate the $qqH \to qqb\bar{b}$ signal from the QCD multijet background for each individual year. The following variables are used as inputs to the BDT:

- Properties of the VBF-tagged jets: invariant mass (m_{jj}), difference in the pseudorapidity ($\Delta\eta_{jj}$), and difference in the azimuthal angle ($\Delta\phi_{jj}$);
- The minimal opening angle between the momentum vector of any of the two VBF-tagged jets and the momentum vector of the dijet system composed by the VBF-tagged jet pair (α_{jj});
- The quark-gluon discriminator [58, 59] score of the two VBF-tagged jets. This is a likelihood discriminator constructed using the information on the charged and the neutral constituents of a given jet and the jet shape variables to distinguish between the jets originating from quarks and from gluons;

- The DEEPJET b-tagging scores of the two selected b-tagged jets assigned to the $H \to b\bar{b}$ decay;
- The ratio of the magnitude of the transverse momentum vector of the selected four-jet system to the scalar p_T-sum of the four selected jets ($|\sum \vec{p}_T| / \sum p_T$);
- The longitudinal component of the momentum vector of the selected four-jet system ($\sum p_z$);
- The difference in the azimuthal angle between the Higgs boson candidate and the dijet system composed of the VBF-tagged jets ($|\phi_{b\bar{b}} - \phi_{jj}|$); and
- The multiplicity and p_T sum of extra jets with $p_T > 30\,\text{GeV}$ and $|\eta| < 2.4$, excluding the selected b-tagged and VBF-tagged jets.

The training is performed using half of the simulated VBF events and 2.5% of the data sample after event selection as a proxy for the dominant QCD multijet background, the rest of the simulated VBF sample as well as another 2.5% of the data is used for the validation of the training. Dedicated studies were performed to assess the impact of using data events in the BDT training. In the first study, several other disjoint data subsets corresponding to 5% of the total sample were employed in the training and validation of the training. In the second study, the subset of data used in the training was removed from the data set used for the extraction of signal. The impact of these alternative analysis strategies on the measured signal rate and its uncertainty was found to be below 2%. Figure 3 shows the distributions of the BDT output score (D) normalized to unity for the VBF, ggH, and $Z \to b\bar{b}$ processes and the data as an approximation to the QCD multijet background in the `Tight 2016` and `Tight 2018` samples.

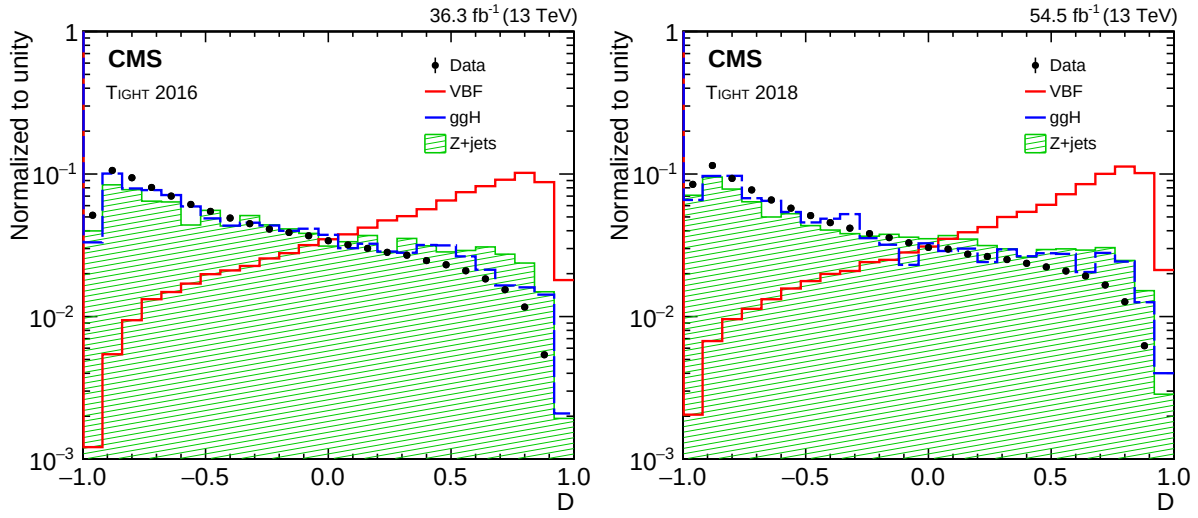

Figure 3: The unit normalized distributions of the VBF BDT outputs in data and simulated samples in the `Tight 2016` (left) and `Tight 2018` (right) analysis samples. Data events (points), dominated by the QCD multijet background, are compared to the VBF (red solid line), ggH (blue dashed line), and Z+jets (green hatched area) processes.

In the `Loose` samples, where larger contributions from ggH and Z+jets events are expected compared to the `Tight` sample, a multiclass BDT is trained to separate four processes simultaneously: (1) VBF Higgs boson production, (2) ggH Higgs boson production, (3) Z+jets, and (4) QCD multijet events. The training is performed using simulated samples of VBF, ggH, and Z+jets events and 5% of the data in the `Loose 2016` and `Loose 2018` samples. The BDTs trained in the `Loose` sample use the same set of input variables as the binary BDT classifiers

trained in the Tight analysis samples. The multiclass BDT has four outputs, D_{VBF}, D_{ggH}, D_{Z}, and D_{QCD}, quantifying the compatibility of each event with the VBF, ggH, Z+jets, and QCD multijet production hypotheses, respectively. The distributions of D_{VBF}, D_{ggH} and D_{Z} normalized to unity are shown in Fig. 4 for data and simulated samples. Better discrimination between the VBF signal and background processes is observed in the Loose 2016 sample compared to the Loose 2018 sample, as visible in the D_{VBF} and D_{Z} distributions, because of the different trigger requirements. These samples contain events failing the HLT_Tight trigger. In 2016 data, the trigger selection on m_{jj} and $\Delta\eta_{\mathrm{jj}}$ is more stringent compared with 2018 data (see Table 1). As a consequence, in the Loose 2018 sample, a larger part of phase space, where m_{jj} and $\Delta\eta_{\mathrm{jj}}$ are particularly sensitive to the VBF signal, is removed in comparison with the Loose 2016 sample, thus making the BDT in the Loose 2018 sample less performant in discrimination between the VBF signal and background processes than in the Loose 2016 sample.

Based on their BDT scores, events are classified into multiple exclusive categories, targeting the VBF, ggH, and Z+jets processes. Details of the event categorization and the naming convention of the event categories are given in Table 2. The BDT thresholds defining each category, are optimized by maximizing the quantity $S/\sqrt{B}$, where S is the number of expected events of the targeted process and B is the number of QCD multijet background events approximated as the observed data events in the $m_{\mathrm{b\bar{b}}}$ interval populated by the targeted process. The $m_{\mathrm{b\bar{b}}}$ interval of 80–100 GeV is used for the Z+jets process and 104–146 GeV for the VBF and ggH processes. In total, 18 categories are introduced, three in each of the two Tight analysis samples, and six in each of the two Loose analysis samples.

The aim of introducing distinct categories sensitive to the production of the Z boson is twofold. Firstly, these categories are intended to establish the signal from the $\mathrm{Z} \to \mathrm{b\bar{b}}$ production, thereby validating the analysis techniques employed in this study. Secondly, the tail of each $m_{\mathrm{b\bar{b}}}$ distribution in the Z+jets sample extends to the region partially populated by the signal events, thus affecting the precision of the measurement. It is therefore important to constrain the background from the Z+jets process with dedicated categories, thus improving the sensitivity to the signal. Further, separate categories targeting the ggH process improves the sensitivity of the analysis to inclusive Higgs boson production.

The numbers of selected events in data along with the expected background and signal yields in each analysis category are detailed in Tables 3 and 4. The signal contribution is significantly smaller than the backgrounds in all analysis categories.

6.4 Signal extraction

The test statistic chosen to determine the signal yield is based on the profile likelihood ratio [60]. The signal is extracted from the simultaneous binned maximum likelihood fit of the $m_{\mathrm{b\bar{b}}}$ distribution in all categories obtained from the data. In each category, the $m_{\mathrm{b\bar{b}}}$ distribution is fitted with a superposition of three parametric analytic functions accounting for: (i) the continuum background, dominated by QCD multijet events, (ii) resonant Z+jets background and, (iii) signal. Contributions from other processes are found to have a negligible effect on the results. The addition of separate templates accounting for the W+jets, $\mathrm{t\bar{t}}$, and $\mathrm{t}/\bar{\mathrm{t}}$ backgrounds, changes the extracted signal yield and its uncertainty by less than 1%. The aggregate contribution from other decays of the Higgs boson ($\mathrm{H} \to \mathrm{c\bar{c}}$, $\mathrm{H} \to \tau\tau$) and from the other production modes ($\mathrm{t\bar{t}H}$ and VH) is evaluated to be almost two orders of magnitude lower than the contributions from the VBF and ggH processes, hence their contributions are neglected in the signal extraction procedure. The expected yields of the VBF, ggH, and Z+jets processes in a given category

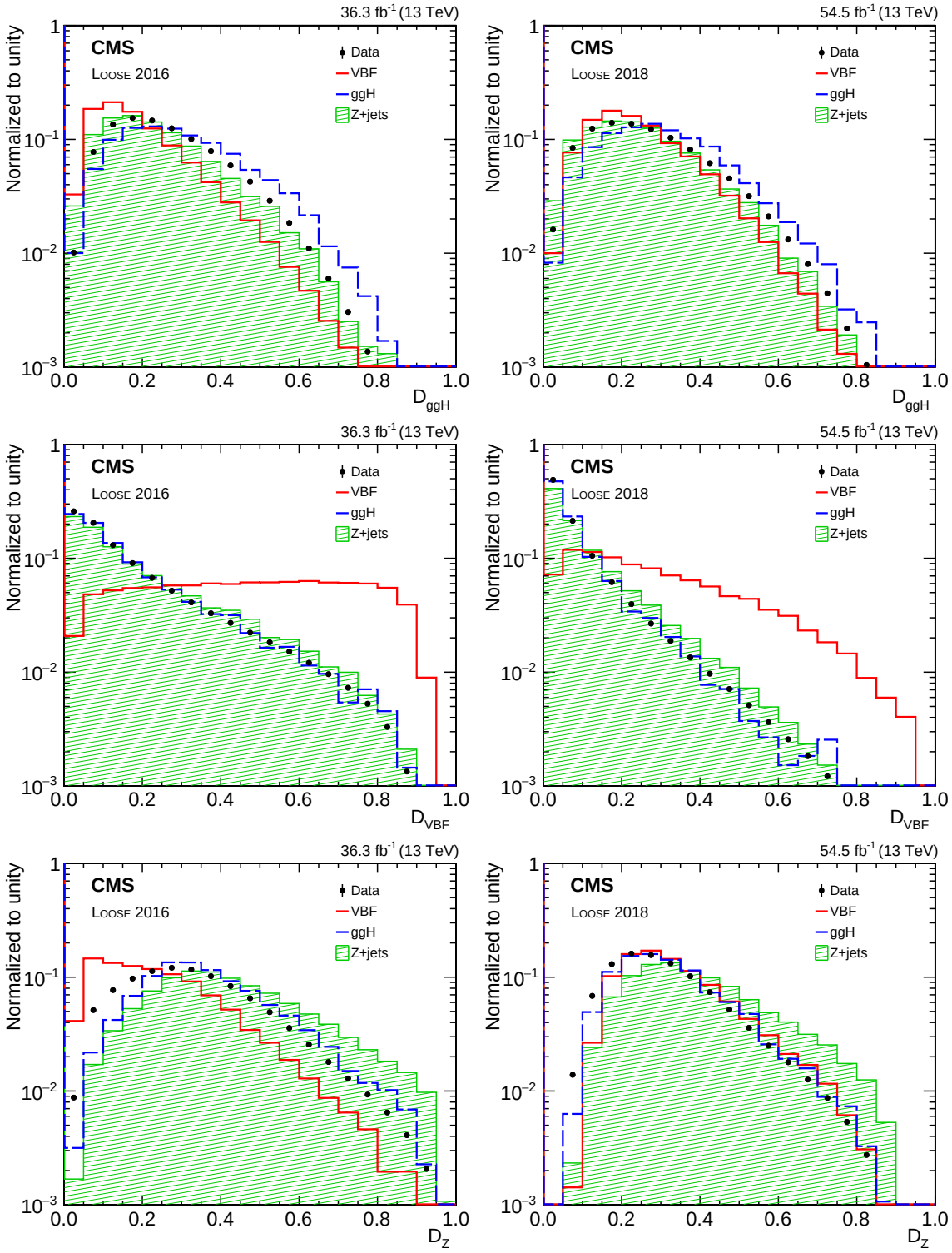

Figure 4: The unit normalized distributions of the BDT outputs: D_{ggH} (upper), D_{VBF} (middle), and D_{Z} (lower) in data and simulated samples in the `Loose 2016` (left) and `Loose 2018` (right) analysis samples. Data events (points), dominated by the QCD multijet background, are compared to the VBF (red solid line), ggH (blue dashed line), and Z+jets (green hatched area) processes.

are estimated from simulation. The $m_{\mathrm{b\bar{b}}}$ distributions for the VBF and ggH signal and Z+jets

Table 2: Event categorization used in the analysis for a total of 18 categories. The names of the categories are given in the first column. The BDT score boundaries defining each category are given in the second column and the targeted process is indicated in the third column.

Category	BDT score boundaries	Targeted process
	2016	
`Tight 1`	$0.25 < D < 0.50$	VBF
`Tight 2`	$0.50 < D < 0.75$	VBF
`Tight 3`	$0.75 < D$	VBF
`Loose G1`	$0.50 < D_{\mathrm{ggH}} < 0.55$	ggH
`Loose G2`	$0.55 < D_{\mathrm{ggH}}$	ggH
`Loose V1`	$D_{\mathrm{ggH}} < 0.50$, $0.80 < D_{\mathrm{VBF}} < 0.85$	VBF
`Loose V2`	$D_{\mathrm{ggH}} < 0.50$, $0.85 < D_{\mathrm{VBF}}$	VBF
`Loose Z1`	$D_{\mathrm{ggH}} < 0.50$, $D_{\mathrm{VBF}} < 0.80$, $0.60 < D_{\mathrm{Z}} < 0.75$	Z+jets
`Loose Z2`	$D_{\mathrm{ggH}} < 0.50$, $D_{\mathrm{VBF}} < 0.80$, $0.75 < D_{\mathrm{Z}}$	Z+jets
	2018	
`Tight 1`	$0.25 < D < 0.50$	VBF
`Tight 2`	$0.50 < D < 0.75$	VBF
`Tight 3`	$0.75 < D$	VBF
`Loose G1`	$0.55 < D_{\mathrm{ggH}} < 0.60$	ggH
`Loose G2`	$0.60 < D_{\mathrm{ggH}}$	ggH
`Loose V1`	$D_{\mathrm{ggH}} < 0.55$, $0.50 < D_{\mathrm{VBF}} < 0.55$	VBF
`Loose V2`	$D_{\mathrm{ggH}} < 0.55$, $0.55 < D_{\mathrm{VBF}}$	VBF
`Loose Z1`	$D_{\mathrm{ggH}} < 0.55$, $D_{\mathrm{VBF}} < 0.50$, $0.60 < D_{\mathrm{Z}} < 0.70$	Z+jets
`Loose Z2`	$D_{\mathrm{ggH}} < 0.55$, $D_{\mathrm{VBF}} < 0.50$, $0.70 < D_{\mathrm{Z}}$	Z+jets

background are individually modeled with a superposition of a one-sided Crystal Ball (CB) function [56] for the resonant part and a second-order Bernstein polynomial accounting for the contribution from events where the jets are misassigned to the decay of the Z or the Higgs boson. The parameters of the CB function and the Bernstein polynomial are extracted from the fit to the $m_{\mathrm{b\bar{b}}}$ spectrum in the respective simulated sample, and separately for each sample. For the signal, as well as the Z+jets processes, the variations of the shapes across the different event categories within the same analysis sample are found to be well within the statistical uncertainties of the MC samples, and significantly smaller than the variations caused by the experimental uncertainties associated with the b jet energy scale and resolution. For the VBF and ggH processes, which have similar shapes, a common analytic function is used to model the $m_{\mathrm{b\bar{b}}}$ distribution in each analysis sample, namely `Tight 2016`, `Loose 2016`, `Tight 2018` and `Loose 2018`. The same approach is pursued for the $\mathrm{q\bar{q}} \to \mathrm{Z}$ and $\mathrm{WW} \to \mathrm{Z}$ processes. Figure 5 illustrates the modeling of the $m_{\mathrm{b\bar{b}}}$ shape in samples of the simulated VBF, ggH, and Z+jets events assigned to the `Tight 2016` analysis sample.

For all analysis samples, the fitted peak positions of the CB functions describing the $m_{\mathrm{b\bar{b}}}$ distribution in signal, are found to be consistent within fit uncertainties with the nominal value of the Higgs boson mass. For the resonant $\mathrm{Z} \to \mathrm{b\bar{b}}$ background, we observe a bias in the peak position of about 3.0–3.5 GeV above the nominal value of the Z boson mass. The effect is caused by the relatively high p_{T} thresholds imposed on jets in the HLT and offline selections.

Table 3: Event yields for various categories of the analyzed 2016 data corresponding to $36.3\,\mathrm{fb}^{-1}$, compared to the expected number of events from the simulated samples of signal and background other than the QCD multijet process. The quoted uncertainties are statistical only.

Category	VBF	ggH	Z+jets	$t\bar{t}$ & $t/\bar{t}$	W+jets	Data
`Loose G1`	4.5 ± 0.2	27.5 ± 1.2	275 ± 16	116.7 ± 2.6	10.6 ± 3.0	41432
`Loose G2`	6.1 ± 0.3	51.6 ± 1.8	407 ± 19	127.3 ± 2.7	8.2 ± 2.4	58895
`Loose V1`	19.9 ± 0.4	2.7 ± 0.4	45 ± 2	10.6 ± 0.8	1.9 ± 1.3	4330
`Loose V2`	17.4 ± 0.4	1.7 ± 0.3	31 ± 5	4.7 ± 0.4	0.5 ± 0.3	1901
`Loose Z1`	9.6 ± 0.3	34.8 ± 1.4	1150 ± 20	226.3 ± 3.3	40.8 ± 6.1	78850
`Loose Z2`	3.1 ± 0.2	14.1 ± 0.7	650 ± 10	199.0 ± 3.0	35.0 ± 5.9	29992
`Tight 1`	92.7 ± 1.0	15.6 ± 1.0	161 ± 8	37.6 ± 1.4	7.7 ± 2.5	29864
`Tight 2`	136.2 ± 1.5	13.9 ± 0.9	151 ± 6	22.5 ± 1.2	4.2 ± 1.4	21831
`Tight 3`	117.3 ± 1.1	6.2 ± 0.7	75 ± 3	5.5 ± 0.5	3.1 ± 1.1	7231

Table 4: Event yields for various categories of the analyzed 2018 data corresponding to $54.5\,\mathrm{fb}^{-1}$, compared to the expected number of events from the simulated samples of signal and background other than the QCD multijet process. The quoted uncertainties are statistical only.

Category	VBF	ggH	Z+jets	$t\bar{t}$ & $t/\bar{t}$	W+jets	Data
`Loose G1`	2.4 ± 0.2	13.5 ± 2.1	137 ± 9	32.4 ± 1.4	2.0 ± 0.5	17296
`Loose G2`	2.9 ± 0.2	24.3 ± 1.5	180 ± 10	33.1 ± 1.4	2.1 ± 0.5	24882
`Loose V1`	6.4 ± 0.3	1.0 ± 0.3	22 ± 3	4.4 ± 0.5	0.5 ± 0.3	1914
`Loose V2`	11.0 ± 0.4	1.7 ± 0.4	25 ± 3	4.7 ± 0.5	0.3 ± 0.2	2453
`Loose Z1`	7.0 ± 0.3	10.8 ± 0.9	506 ± 10	59.0 ± 1.7	19.5 ± 2.7	24559
`Loose Z2`	4.0 ± 0.2	7.1 ± 0.7	445 ± 7	99.0 ± 2.2	24.0 ± 2.8	14530
`Tight 1`	89.5 ± 1.1	18.0 ± 3.2	190 ± 8	49.3 ± 1.5	8.0 ± 2.5	29261
`Tight 2`	139.8 ± 1.4	17.9 ± 3.3	202 ± 7	31.6 ± 1.3	7.2 ± 2.4	23392
`Tight 3`	134.5 ± 1.4	8.7 ± 2.6	104 ± 5	7.6 ± 0.6	3.4 ± 1.6	8202

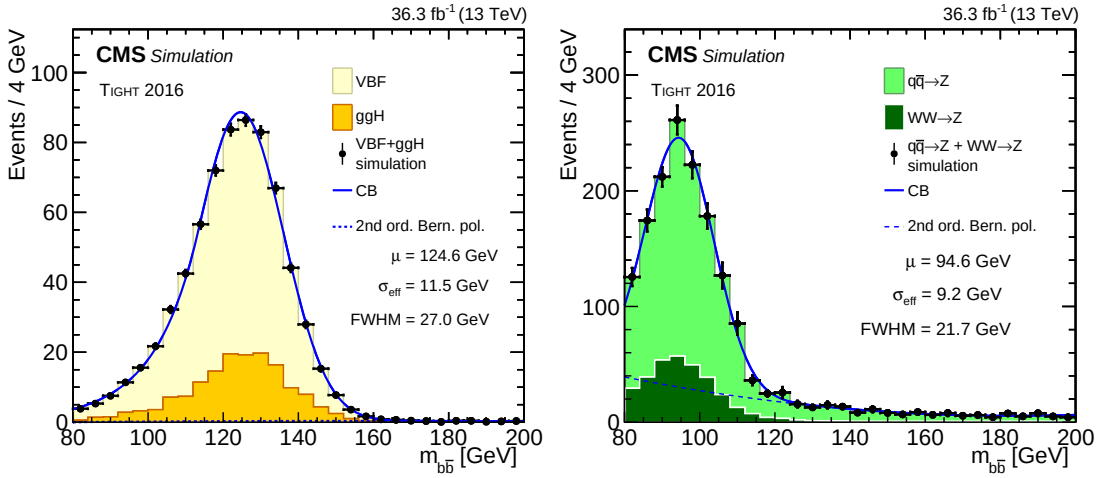

Figure 5: The $m_{b\bar{b}}$ distributions from simulation with overlaid parametric fits (solid blue lines) for the `Tight 2016` analysis sample. Left: The fitted $m_{b\bar{b}}$ distribution in the signal combining the VBF (yellow histogram) and ggH (orange) contributions. The black points refer to the total Higgs boson contribution from VBF and ggH production modes. Right: The fitted $m_{b\bar{b}}$ distribution in simulated Z+jets background (black points) combining the WW $\to$ Z (dark green histogram) and $q\bar{q}$ $\to$ Z (light green histogram) production modes. The black points refer to the total Z+jets contribution from $q\bar{q}$ $\to$ Z and WW $\to$ Z modes. The dotted lines represent the second-order Bernstein polynomial components used to approximate the contributions from the wrong jet pairing.

These thresholds, optimized primarily for the selection of H $\to$ $b\bar{b}$ decays, result in an upward shift of the peak position in the Z $\to$ $b\bar{b}$ sample, where a larger fraction of low-p_T b jets is expected compared to H $\to$ $b\bar{b}$ decays. A dedicated simulation study has demonstrated that no bias is present in the Z $\to$ $b\bar{b}$ sample if no trigger requirements are applied as well as if jet p_T thresholds are relaxed in the offline selection.

The shape and normalization of the continuum background are estimated from the fit to data. The shape of the continuum background is modeled individually in each event category i by a product of exponential and polynomial functions of order n,

$$F_i^{\mathrm{QCD}} = \exp\left(-b_i m_{b\bar{b}}\right)\left(1+\sum_{j=1}^{n} a_{ij} m_{b\bar{b}}^{j}\right). \quad (1)$$

The family of functions given by Eq. (1) includes the case corresponding to the zeroth order polynomial. In each category, the choice of the polynomial function is guided by the combined fit of two sideband regions, $80 < m_{b\bar{b}} < 104\,\mathrm{GeV}$ and $146 < m_{b\bar{b}} < 200\,\mathrm{GeV}$. Sequential fits with increasing polynomial order are performed followed by a Fisher F-test [61] to select the function with the fewest number of parameters necessary to fit the data. The contribution from the Z+jets background is accounted for by performing fits with the superposition of two functions,

- tested analytic function from the family defined by Eq. 1 modeling continuum background dominated by the QCD multijet process;
- and a combination of the CB function and a second order Bernstein polynomial for the Z+jets background as described earlier in this section.

First, the selection of functions for the modeling of the continuum background is performed in the categories targeting the Z+jets process: `Loose Z1` and `Loose Z2` in the 2016 and 2018 samples. Fits in each of the four aforementioned categories are performed by varying the normalization of the Z+jets process in an unconstrained manner. An additional degree of freedom is introduced to account for the unconstrained normalization of the Z+jets process. A dedicated statistical test demonstrated that the measured normalizations of the Z+jets process across the four categories are consistent. The p-value quantifying the compatibility of these measurements is found to be 0.33. Once the functional form of the continuum background modeling in each category targeting the Z+jets process is selected based on the F-test result, a combined fit is performed in these four categories with a common, unconstrained Z+jets normalization parameter.

The selection of functions from the family given in Eq. 1 in the categories targeting VBF and ggH processes is done by performing fits with a Gaussian constraint imposed on the normalization of the Z+jets component. This constraint is obtained from the combined fit in the four categories targeting the Z+jets process.

Ideally, the final result should not depend on the choice of the parametric fit function, but in reality, the choice of the function to model the background may bias the extraction of the signal. Therefore, a dedicated study is performed for each category to assess a possible bias in the signal extraction. For each of the selected functions, various alternative models of the continuum background are used to generate an ensemble of pseudo-data, including the injected signal and the contribution from Z+jets process. The resulting $m_{\mathrm{b\bar{b}}}$ spectra obtained from the pseudo-data are fitted using the nominal model of the continuum background and the distribution of the extracted signal yield is compared to the injected yield. The study is performed using the following alternative models:

1. Functions from the same family, given by Eq. (1), but with polynomials one or two orders higher than the nominal function.

2. Inverse polynomials, $I(m_{\mathrm{b\bar{b}}}) = 1/(1 + \sum_{j=1}^{n} a_j m_{\mathrm{b\bar{b}}}^{j})$, with $n = 2$ or 3.

The injected signal yield is varied between 50–200% of the yield predicted by the SM to investigate a possible dependence of the bias on the signal strength. The background model chosen yields a maximum potential bias that does not exceed 10% of the statistical uncertainty on the fitted signal rate in each individual event category, and has negligible impact on the measurement. The systematic uncertainty related to the choice of the function used to model the continuum background has a subdominant effect on the final results. The functional forms employed in the modeling of the continuum background in each event category are reported in Table 5.

7 Systematic uncertainties

Several systematic uncertainties affect the overall normalizations and shapes of the $m_{\mathrm{b\bar{b}}}$ distributions for signal and background. Systematic uncertainties are incorporated in the signal extraction procedure via nuisance parameters with Gaussian or log-normal probability density functions (pdfs), which are treated according to the frequentist paradigm. These pdfs are included as additional factors in the likelihood function, which is maximized in the fit. All uncertainties are divided into two categories. Theoretical uncertainties arise from the limited

Table 5: The functional forms used to fit the continuum component of the background in various analysis categories. The notation "exp" stands for the exponential function, "exp·pol1 (pol2)" denotes the product of an exponential function and a first-order (second-order) polynomial.

Category	Samples	
	Loose 2016	Loose 2018
G1	exp·pol2	exp·pol1
G2	exp·pol2	exp·pol1
V1	exp	exp
V2	exp	exp
Z1	exp·pol1	exp·pol1
Z2	exp·pol1	exp·pol1
	Tight 2016	Tight 2018
1	exp	exp
2	exp	exp
3	exp	exp

precision in the computation of the inclusive and differential cross sections of the modeled processes and are fully correlated between event categories and data-taking periods. Experimental uncertainties comprise (i) uncertainties related to the imperfect simulation of the detector response and consequent inaccurate modeling of the reconstruction of physics objects and observables in the simulated samples, (ii) the uncertainty in the integrated luminosity estimation, and (iii) the uncertainty in the modeling of the pileup interactions. The dominant uncertainties affecting this measurement are briefly summarized in the following.

Theoretical uncertainties

- *Parton shower uncertainty in* PYTHIA: The uncertainty related to the modeling of the parton shower in PYTHIA is estimated by varying the scales of the initial- and final-state QCD radiation. This uncertainty has a sizable effect on modeling of jet-related variables used as inputs to the BDT, thereby affecting acceptance of signal and background events in different event categories. The impact on the predicted event yields varies between 2 and 10% across event categories with larger effects observed for categories targeting VBF production. The modeling of key BDT input variables, such as m_{jj} and $\Delta\eta_{jj}$, is validated with a control sample of events, in which a Z boson is produced in association with at least two jets and decays into a pair of muons. Distributions of these variables in data and simulated samples agree within instrumental and theoretical uncertainties, including the uncertainty related to the modeling of the parton shower in PYTHIA. Variations in the $m_{b\bar{b}}$ distribution within these uncertainties are found to be negligible in the simulated signal and Z+jets background samples. Inclusion of these shape-altering effects in the statistical inference procedure changes the uncertainty in the extracted rates of the signal and resonant $Z \to b\bar{b}$ background by less than 0.5%.
- *Parton shower and hadronization model for VBF production*: Simulation of the color connection between the incoming and outgoing partons in the VBF process is particularly sensitive to the choice of the event generator. The related uncertainty is assessed by comparing the dipole parton shower model implemented in PYTHIA with the alternative one provided by the HERWIG event generator. Yields of the VBF sig-

nal in each event category are compared between the two models and the differences are used to define a double-sided uncertainty with the PYTHIA prediction taken as the central estimate. The choice of the event generator only marginally affects the shapes of the $m_{b\bar{b}}$ distributions in different event categories. The corresponding shape variations in the $m_{b\bar{b}}$ spectra modify the expected uncertainty in the extracted rate of the VBF process by less than 1%. The choice of the generator also impacts the simulation of forward jets in the WW $\rightarrow$ Z sample. The validation study performed using the control sample of Z boson decays into muons, described above, demonstrates that properties of spectator jets accompanying the production of a Z boson, are well modeled by PYTHIA. Small discrepancies between data and simulation observed in distributions of key variables are fully covered by variations of the scales of the initial- and final-state QCD radiation. Therefore, no additional uncertainty is assigned to the parton shower modeling in the simulated WW $\rightarrow$ Z sample.

- *Scale variations*: Uncertainties arising from missing higher-order QCD corrections in the theoretical computations affect the overall production rates as well as the kinematics of the simulated processes. The impact of these uncertainties on the cross sections of the VBF and the ggH productions are estimated by varying the renormalization and factorization scales, yielding uncertainties of $\pm 2.1\%$ and $^{+4.6}_{-6.7}\%$, respectively [11]. The impact on the acceptance of VBF and ggH events across the event categories is evaluated by applying event weights that reflect the effect of the scale variations on the kinematics of the simulated events. The variations in event yields across categories are typically between 1 and 4%, with larger effects observed in categories targeting the VBF process.
- *Uncertainties in PDFs and α_S*: The PDF and α_S uncertainties in the cross sections of the VBF and ggH processes are $\pm 0.4\%$ and $\pm 3.2\%$, respectively [11].
- *Uncertainty in the branching fraction*: The theoretical uncertainty in the branching fraction of the Higgs boson decay to bottom quarks is 0.65% at $m_H = 125\,\text{GeV}$ [11].
- *Uncertainties from Z+jets NLO K-factors*: The MC samples of $q\bar{q} \rightarrow Z$ and WW $\rightarrow$ Z events are simulated with MADGRAPH5_aMC@NLO at the LO accuracy with MLM matching. To improve the modeling of these processes, additional p_T-dependent *K*-factors are applied following the prescription in Ref. [46] to match the differential distribution of the Z boson p_T as predicted by the NNLO QCD and NLO EW calculations. The *K*-factors related to the NLO EW corrections are applied to both $q\bar{q} \rightarrow Z$ and WW $\rightarrow$ Z samples. The *K*-factors associated with the NNLO QCD corrections are applied only to the $q\bar{q} \rightarrow Z$ sample. The uncertainties in these *K*-factors are incorporated via six nuisance parameters. Three of these nuisance parameters correspond to the NLO EW corrections and affect both $q\bar{q} \rightarrow Z$ and WW $\rightarrow$ Z samples, whereas another three parameters are related to the NNLO QCD corrections and have an impact only on simulated $q\bar{q} \rightarrow Z$ events. Variations of these nuisance parameters change the acceptance of Z+jets events in different event categories by 1–7%. Uncertainties related to missing higher order QCD corrections in the simulated WW $\rightarrow$ Z sample are evaluated by varying renormalization and factorization QCD scales, modifying the acceptance of Z+jets events by 1–3% across different event categories.

Experimental uncertainties

- *Jet energy scale and resolution corrections*: The uncertainties in the jet energy scale and resolution originate from different sources with limited correlations [28, 59]. The

uncertainties depend on the jet kinematics and are typically larger in the forward regions. Variations of the jet four-momenta caused by these uncertainties have an impact on the acceptance in various event categories of between 5 and 10%.

- *b tagging*: The uncertainties in b tagging efficiency are evaluated with the control samples of the semileptonic $t\bar{t}$ decays, Z+jets events, and the inclusive QCD multijet events [30]. The uncertainties associated with the selection of the working point of the DEEPJET score for the tagger vary between 4–8% depending on jet flavor, p_T, and η. The DEEPJET discriminants of the two b-tagged jets are also used as an input to the BDT classifiers. An assessment of control samples of QCD multijet and leptonic $t\bar{t}$ events revealed only small differences in the DEEPJET discriminant distribution between data and simulated events above the threshold defining the working point. These differences are found to have subdominant effects on the response of BDT classifiers, leading to a migration of events between categories at a percent level.
- *Trigger efficiency*: The corrections to the trigger efficiency are discussed in Section 5. The uncertainties in the trigger scale factors are predominantly statistical. The impact of these uncertainties on the acceptance of signal and background events in various analysis categories is estimated to range from 5 to 10%.
- *Corrections to b jet energy regression*: The scale and smearing corrections to the regressed b jet energy are derived as described in Section 6.2. The uncertainties in the corrections are propagated to the parameters of the CB functions modeling the core of the $m_{b\bar{b}}$ spectrum in the simulated samples of $H \to b\bar{b}$ and $Z \to b\bar{b}$ decays. Furthermore, these uncertainties change the shape of several observables used as inputs to the BDT classifiers, and consequently affect the estimate of the acceptance in various event categories.
- *Integrated luminosity*: The uncertainty in the luminosity measurement has both correlated and uncorrelated components, which vary across different data-taking periods [62, 63]. The uncertainties of the individual years are 1.2 and 2.5% for 2016 and 2018, respectively. The uncertainty of the combined 2016 and 2018 integrated luminosity is 1.7% (calculated using the full correlation scheme and per-year luminosities of 36.3 fb^{-1} and 54.5 fb^{-1}, respectively).
- *Pileup modeling*: The number of primary interactions per bunch crossing varies with the instantaneous luminosity during the data-taking operation. In order to match the distribution of pileup in data with that in the simulated samples, weights are applied that are determined by studying minimum-bias data sets. A normalization uncertainty is derived by altering the pileup weights obtained by changing the total inelastic cross section by $\pm 4.6\%$ [64] of its nominal value.
- *Pileup jet identification*: This uncertainty is estimated by comparing the pileup jet identification score [54] in events with a Z boson decaying into a pair of electrons or muons and one balanced jet in data and simulation. The assigned uncertainty depends on p_T and $|\eta|$, and is designed to cover all differences between data and simulation in the distribution.

The impact of the most significant uncertainties is presented in Table 6.

8 Results

This analysis is primarily sensitive to the VBF Higgs boson production followed by $H \to b\bar{b}$ decay. The outcome of the measurement depends on how the contribution from the ggH pro-

Table 6: The impact of the dominant systematic uncertainties on the observed signal strength for inclusive Higgs boson production followed by decay to bottom quarks.

Source of systematic uncertainty	Impact on signal strength [%]
VBF parton shower	13.0
Jet energy scale	7.7
Trigger efficiency	6.7
Parton shower (final-state radiation)	5.6
b jet regression smearing	3.3
b tagging efficiency	3.0
Pileup modeling	2.3
b jet regression scale	2.0
Jet energy resolution	1.5

cess is accounted for, and three scenarios are presented that differ in the way this process is treated in the signal extraction procedure. In each scenario, the best fit value of the parameters of interest and their confidence level (CL) intervals are extracted following the procedure described in Section 3.2 of Ref. [65].

8.1 Measurement of inclusive Higgs boson production

In the measurement of the inclusive Higgs boson production rate, the ggH process is considered as part of the signal. The fit is performed with an unconstrained signal strength modifier $\mu^{\text{incl.}}_{\text{Hb}\bar{\text{b}}}$ that simultaneously scales the yields of VBF and ggH events in all categories. The parameter $\mu^{\text{incl.}}_{\text{Hb}\bar{\text{b}}}$ is the product of the inclusive production cross section of the Higgs boson and the $\text{H} \to \text{b}\bar{\text{b}}$ branching fraction relative to the SM expectation. In the measurement, we allow the overall normalization of the Z+jets process $\mu_{\text{Zb}\bar{\text{b}}}$ to vary in an unconstrained manner.

The analytic function used to fit the $m_{\text{b}\bar{\text{b}}}$ spectrum in the ith category is given by

$$\begin{aligned} F_i(m_{\text{b}\bar{\text{b}}}|\vec{\theta}) = N_i^{\text{QCD}} F_i^{\text{QCD}}(m_{\text{b}\bar{\text{b}}}|\vec{\alpha}_i) + \mu_{\text{Zb}\bar{\text{b}}} N_i^{\text{Zb}\bar{\text{b}}}(\vec{\theta}) F_i^{\text{Zb}\bar{\text{b}}}(m_{\text{b}\bar{\text{b}}}|\vec{\theta}_S) \\ + \mu^{\text{incl.}}_{\text{Hb}\bar{\text{b}}}(N_i^{\text{qqH}}(\vec{\theta}) + N_i^{\text{ggH}}(\vec{\theta})) F_i^{\text{Hb}\bar{\text{b}}}(m_{\text{b}\bar{\text{b}}}|\vec{\theta}_S). \end{aligned} \tag{2}$$

The function includes the following category-dependent components:

- N_i^{QCD}: the normalization of the QCD multijet background extracted from the fit.
- $F_i^{\text{QCD}}(m_{\text{b}\bar{\text{b}}}|\vec{\alpha}_i)$: analytic parametric function normalized to unity modeling the shape of the QCD multijet background. The parameters $\vec{\alpha}_i$ of the function are obtained from the fit. The types of functions used to model the QCD multijet background are discussed in Section 6.4.
- $N_i^{\text{qqH,ggH,Zb}\bar{\text{b}}}(\vec{\theta})$: predicted yields of the VBF, ggH, and Z+jets processes; these yields depend on the nuisance parameters $\vec{\theta}$ that incorporate systematic uncertainties in the fit.
- $F_i^{\text{Hb}\bar{\text{b}},\text{Zb}\bar{\text{b}}}(m_{\text{b}\bar{\text{b}}}|\vec{\theta}_S)$: analytic functions normalized to unity modeling the shape of the $m_{\text{b}\bar{\text{b}}}$ distribution in the samples of $\text{H} \to \text{b}\bar{\text{b}}$ and $\text{Z} \to \text{b}\bar{\text{b}}$ decays. The parameters of the analytic functions, described in Section 6.4, are influenced by the nuisance parameters $\vec{\theta}_S$ associated with the uncertainties in the scale and resolution of the b jet energy regression.

The measurement of the inclusive Higgs boson production yields the best fit values as

$$\mu^{\text{incl.}}_{\text{Hb}\bar{\text{b}}} = 0.99^{+0.32}_{-0.20}\,(\text{syst}) \pm 0.36\,(\text{stat}), \quad \text{and}$$
$$\mu_{\text{Zb}\bar{\text{b}}} = 0.96 \pm 0.21\,(\text{syst}) \pm 0.23\,(\text{stat}).$$

The $\text{H} \to \text{b}\bar{\text{b}}$ signal, including contributions from the VBF and ggH processes, is observed with a statistical significance of $2.6\,\sigma$, compared to the expected significance of $2.9\,\sigma$. The sensitivity of the measurement is driven by the `Tight` categories, while the `Loose` categories constrain the Z+jets background. The expected uncertainty in $\mu^{\text{incl.}}_{\text{Hb}\bar{\text{b}}}$ is determined from the fit to the Asimov dataset [66], where cross sections of the Z and Higgs boson production are set to the values predicted by the SM, whereas parameters of pdfs describing the continuum background, are set to the values obtained from fits to sideband regions. The expected systematic and statistical uncertainties are both found to be about 10% smaller than the respective observed ones. As a consequence, the expected significance is about 10% higher than the observed one, despite the central observed value of $\mu^{\text{incl.}}_{\text{Hb}\bar{\text{b}}}$ being close to unity. The linear correlation coefficient between $\mu^{\text{incl.}}_{\text{Hb}\bar{\text{b}}}$ and $\mu_{\text{Zb}\bar{\text{b}}}$ is found to be 0.37. In the fit, yields of $\text{H} \to \text{b}\bar{\text{b}}$ and $\text{Z} \to \text{b}\bar{\text{b}}$ events are both anti-correlated with the yield of a large continuum background. Hence, a positive correlation between $\mu^{\text{incl.}}_{\text{Hb}\bar{\text{b}}}$ and $\mu_{\text{Zb}\bar{\text{b}}}$ is expected and confirmed by the fit result.

Figures 6 and 7 show the results of the fit in the `Tight 2016` and `Tight 2018` categories, and Fig. 8 is for the `Loose 2016 Z2` and `Loose 2018 Z2` categories. In these Figures, χ^2 quantifies the consistency of the $m_{\text{b}\bar{\text{b}}}$ distribution observed in data with the fitted parametric analytic function, ndf is the number of degrees of freedom in the fit, and the p-value is defined as the probability of observing the χ^2 value larger than the actual one.

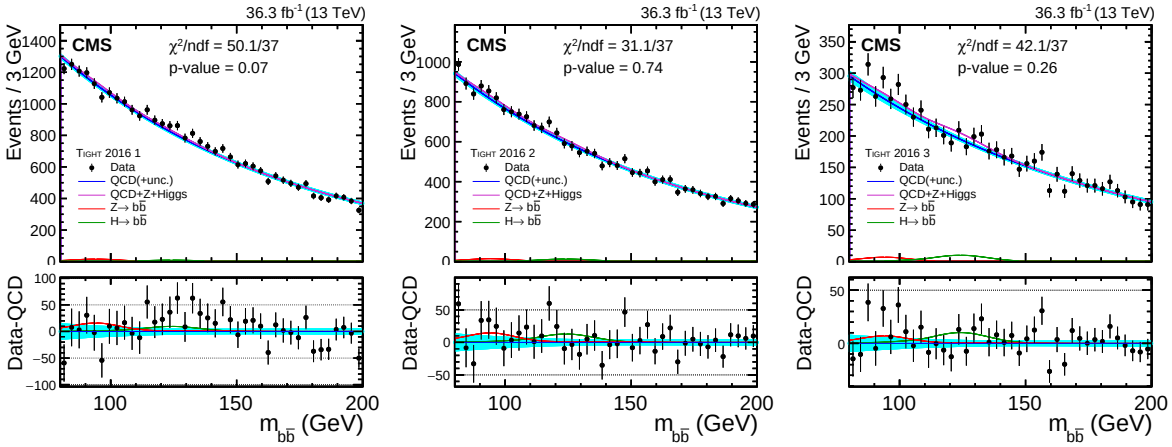

Figure 6: The $m_{\text{b}\bar{\text{b}}}$ distributions in three event categories: `Tight 2016 1` (left), `Tight 2016 2` (center), and `Tight 2016 3` (right). The black points indicate data, the blue solid curve corresponds to the fitted nonresonant component of the background, dominated by QCD multijet events, and the shaded (cyan) band represents the $\pm 1\,\sigma$ uncertainty band. The total signal-plus-background model includes contributions from $\text{Z} \to \text{b}\bar{\text{b}}$, $\text{H} \to \text{b}\bar{\text{b}}$, and the nonresonant component; it is represented by the magenta curve. The lower panel compares the distribution of the data after subtracting the nonresonant component with the resonant contributions of the $\text{Z} \to \text{b}\bar{\text{b}}$ background (red curve) and $\text{H} \to \text{b}\bar{\text{b}}$ signal (green curve).

Figure 9 shows the $m_{\text{b}\bar{\text{b}}}$ spectrum combining all 18 analysis categories. Each category enters the combination with a weight $S/(S+B)$, where S is the total $\text{H} \to \text{b}\bar{\text{b}}$ signal yield (VBF and

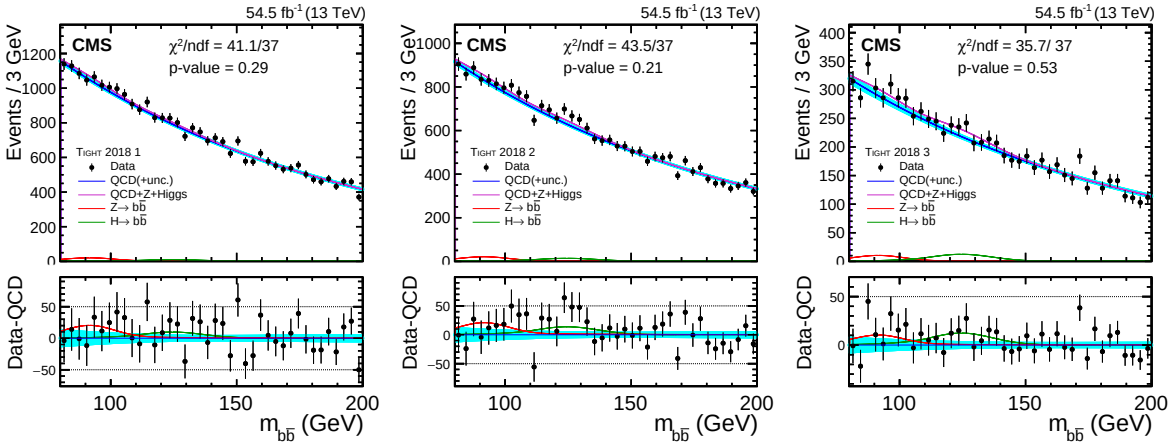

Figure 7: The $m_{b\bar{b}}$ distributions in three event categories: `Tight 2018 1` (left), `Tight 2018 2` (center), and `Tight 2018 3` (right). A complete description is given in Fig. 6.

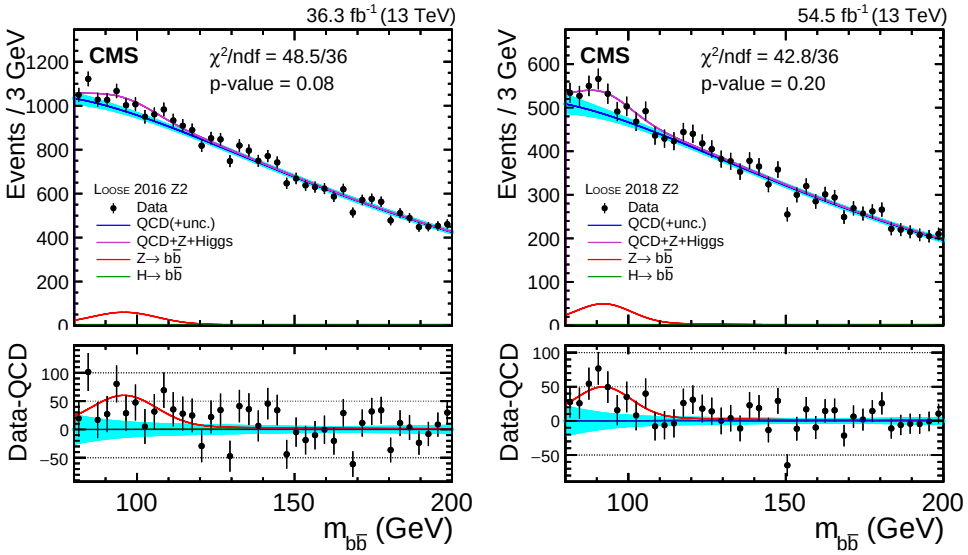

Figure 8: The $m_{b\bar{b}}$ distributions in two event categories: `Loose 2016 Z2` (left) and `Loose 2018 Z2` (right). A complete description is given in Fig. 6.

ggH contributions) and B is the total background yield including QCD multijet and Z+jets processes obtained in a given category from the combined fit. The yields are computed by integrating the $m_{b\bar{b}}$ distribution over the entire fitted range of 80–200 GeV. The distribution in data is compared with the fitted background-only model and the signal-plus-background model.

8.2 Measurement of VBF production when ggH production is constrained to SM expectations

The measurement of the exclusive VBF production rate is performed with the contribution from the ggH process constrained within theoretical and experimental uncertainties to the SM expectation. In this case, the analytic function employed to fit the $m_{b\bar{b}}$ spectrum in category i

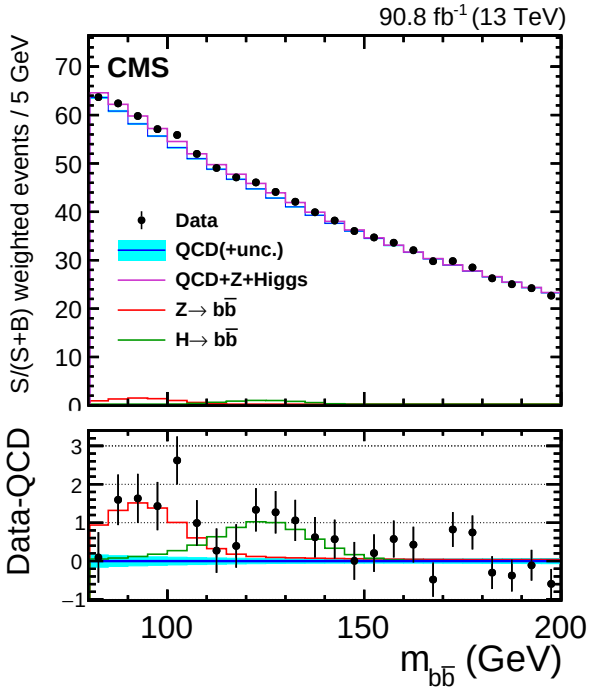

Figure 9: The $m_{\mathrm{b\bar{b}}}$ distribution after weighted combination of all categories in the analysis weighted with $S/(S+B)$. A complete description is given in Fig. 6.

is modified to be

$$F_i(m_{\mathrm{b\bar{b}}}|\vec{\theta}) = N_i^{\mathrm{QCD}} F_i^{\mathrm{QCD}}(m_{\mathrm{b\bar{b}}}|\vec{\alpha}_i) + \mu_{\mathrm{Zb\bar{b}}} N_i^{\mathrm{Zb\bar{b}}}(\vec{\theta}) F_i^{\mathrm{Zb\bar{b}}}(m_{\mathrm{b\bar{b}}}|\vec{\theta}_S) + (\mu_{\mathrm{Hb\bar{b}}}^{\mathrm{qqH}} N_i^{\mathrm{qqH}}(\vec{\theta}) + N_i^{\mathrm{ggH}}(\vec{\theta})) F_i^{\mathrm{Hb\bar{b}}}(m_{\mathrm{b\bar{b}}}|\vec{\theta}_S). \quad (3)$$

The fit is performed with two unconstrained parameters: the signal strength modifier for the VBF process ($\mu_{\mathrm{Hb\bar{b}}}^{\mathrm{qqH}}$) and $\mu_{\mathrm{Zb\bar{b}}}$. The measurement yields

$$\mu_{\mathrm{Hb\bar{b}}}^{\mathrm{qqH}} = 1.01^{+0.39}_{-0.24}\,(\mathrm{syst}) \pm 0.39\,(\mathrm{stat}), \quad \text{and}$$
$$\mu_{\mathrm{Zb\bar{b}}} = 0.96 \pm 0.21\,(\mathrm{syst}) \pm 0.23\,(\mathrm{stat}).$$

The VBF signal is observed with a significance of $2.4\,\sigma$. The expected significance is $2.7\,\sigma$. The best fit values of the signal strength modifiers for the different processes are also shown in Fig. 10.

8.3 Independent measurement of VBF and ggH production

Independent measurement of the VBF and ggH production rates is performed by fitting the $m_{\mathrm{b\bar{b}}}$ spectra with three unconstrained parameters, $\mu_{\mathrm{Zb\bar{b}}}$, $\mu_{\mathrm{Hb\bar{b}}}^{\mathrm{qqH}}$, and $\mu_{\mathrm{Hb\bar{b}}}^{\mathrm{ggH}}$, with the last one being the signal strength for the ggH process. In this measurement, the $m_{\mathrm{b\bar{b}}}$ spectrum in the ith category is fitted with the function

$$F_i(m_{\mathrm{b\bar{b}}}|\vec{\theta}) = N_i^{\mathrm{QCD}} F_i^{\mathrm{QCD}}(m_{\mathrm{b\bar{b}}}|\vec{\alpha}_i) + \mu_{\mathrm{Zb\bar{b}}} N_i^{\mathrm{Zb\bar{b}}}(\vec{\theta}) F_i^{\mathrm{Zb\bar{b}}}(m_{\mathrm{b\bar{b}}}|\vec{\theta}_S) + (\mu_{\mathrm{Hb\bar{b}}}^{\mathrm{qqH}} N_i^{\mathrm{qqH}}(\vec{\theta}) + \mu_{\mathrm{Hb\bar{b}}}^{\mathrm{ggH}} N_i^{\mathrm{ggH}}(\vec{\theta})) F_i^{\mathrm{Hb\bar{b}}}(m_{\mathrm{b\bar{b}}}|\vec{\theta}_S). \quad (4)$$

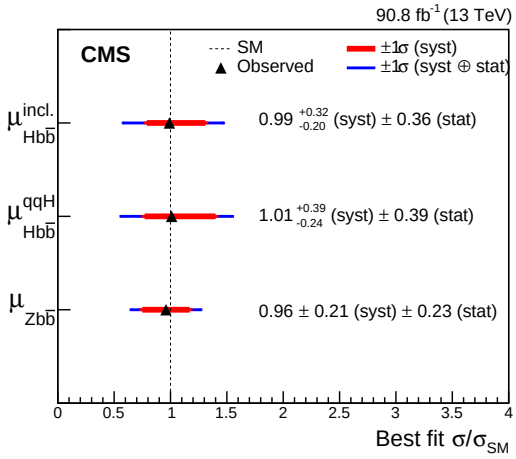

Figure 10: The best fit values of the signal strength modifier for the different processes. The horizontal bars in blue and red colors represent the $\pm 1\,\sigma$ total uncertainty and its systematic component. The vertical dashed line shows the standard model prediction.

The fit yields

$$\mu^{\mathrm{qqH}}_{\mathrm{Hb\bar{b}}} = 1.59^{+0.63}_{-0.72}\,(\mathrm{syst}) \pm 0.54\,(\mathrm{stat}),$$
$$\mu^{\mathrm{ggH}}_{\mathrm{Hb\bar{b}}} = -2.7^{+5.6}_{-2.1}\,(\mathrm{syst}) \pm 3.5\,(\mathrm{stat}), \quad \text{and}$$
$$\mu_{\mathrm{Zb\bar{b}}} = 0.94 \pm 0.20\,(\mathrm{syst}) \pm 0.26\,(\mathrm{stat}).$$

The best fit values of the signal strength modifiers for the different processes are shown in Fig. 11 (left). The negative best fit value for the signal strength modifier of the ggH process, i.e., $\mu^{\mathrm{ggH}}_{\mathrm{Hb\bar{b}}}$, is caused by deficit of the data compared to the expected yields from the background processes only for $m_{\mathrm{b\bar{b}}}$ between 100 and 150 GeV, observed in some of the event categories targeting the ggH or Z+jets processes. A two-dimensional likelihood scan of $\mu^{\mathrm{qqH}}_{\mathrm{Hb\bar{b}}}$ and $\mu^{\mathrm{ggH}}_{\mathrm{Hb\bar{b}}}$ presented in Fig. 11 (right), shows that the measured value of $\mu^{\mathrm{ggH}}_{\mathrm{Hb\bar{b}}}$ is consistent with the SM prediction within $1\,\sigma$. Because of the degeneracy of the $m_{\mathrm{b\bar{b}}}$ distribution shapes in the VBF and ggH processes and the nonnegligible contribution from the ggH process in the categories targeting VBF production, $\mu^{\mathrm{qqH}}_{\mathrm{Hb\bar{b}}}$ and $\mu^{\mathrm{ggH}}_{\mathrm{Hb\bar{b}}}$ exhibit strong anticorrelation with a linear correlation coefficient of -0.63. As a consequence, a downward shift in the measured value of $\mu^{\mathrm{ggH}}_{\mathrm{Hb\bar{b}}}$ causes an upward shift in the measured value of $\mu^{\mathrm{qqH}}_{\mathrm{Hb\bar{b}}}$.

9 Summary

A measurement of the Higgs boson (H) production via vector boson fusion (VBF) process and its decay to a bottom quark-antiquark pair ($\mathrm{b\bar{b}}$) was performed on proton-proton collision data sets collected by the CMS experiment at $\sqrt{s} = 13$ TeV corresponding to a total integrated luminosity of $90.8\,\mathrm{fb}^{-1}$. The analysis employs boosted decision trees (BDTs) to discriminate the signal against major background processes: QCD-induced multijet production and Z+jets events. The BDTs exploit kinematic properties of the VBF jets, information of the b-tagged jets assigned to the $\mathrm{H} \to \mathrm{b\bar{b}}$ decay, and global event shape variables. Based on the BDT response, multiple event categories are introduced, targeting the VBF, gluon-gluon fusion (ggH), and Z+jets pro-

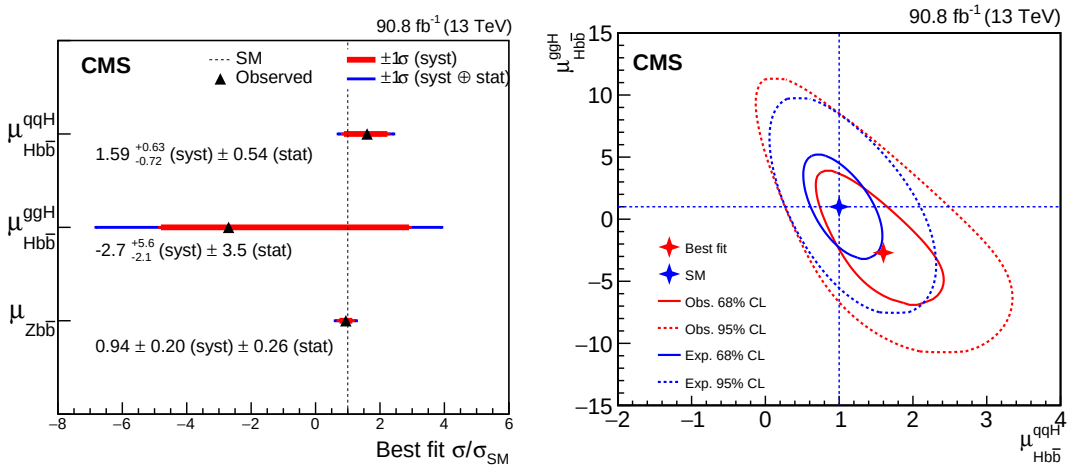

Figure 11: The best fit values of the signal strength modifier for the different processes, the horizontal bars in blue and red colors represent the $\pm 1\,\sigma$ total uncertainty and its systematic component and the vertical dashed line shows the SM prediction (left). The two-dimensional likelihood scan of $\mu^{\mathrm{qqH}}_{\mathrm{Hb\bar{b}}}$ and $\mu^{\mathrm{ggH}}_{\mathrm{Hb\bar{b}}}$, the red (blue) solid and dashed lines correspond to the observed (expected) 68 and 95% CL contours in the $(\mu^{\mathrm{qqH}}_{\mathrm{Hb\bar{b}}}, \mu^{\mathrm{ggH}}_{\mathrm{Hb\bar{b}}})$ plane (right). The SM predicted and observed best fit values are indicated by the blue and red crosses.

cesses to achieve a maximum sensitivity for the signal. While the VBF categories have the highest signal-to-background ratio, the Z+jets categories constrain the largest resonant background. The ggH categories enhance the sensitivity to the inclusive production of the Higgs boson in association with two jets.

The VBF Higgs boson production rate has been measured in its decay to bottom quark-antiquark pairs with the ggH contribution constrained within the theoretical and experimental uncertainties to the standard model prediction. The signal strength of the VBF Higgs production, followed by the $\mathrm{H} \to \mathrm{b\bar{b}}$ decay, defined as the rate of the signal process relative to the value predicted in the standard model, is measured to be, $\mu^{\mathrm{qqH}}_{\mathrm{Hb\bar{b}}} = 1.01^{+0.55}_{-0.46}$. The signal was observed with a significance of 2.4 standard deviations, compared to the expected significance of 2.7 standard deviations. In addition, inclusive Higgs boson production in association with two jets, followed by $\mathrm{H} \to \mathrm{b\bar{b}}$ decay, was measured by treating the ggH contribution as part of the signal. The inclusive signal strength was measured to be $\mu^{\mathrm{incl.}}_{\mathrm{Hb\bar{b}}} = 0.99^{+0.48}_{-0.41}$, corresponding to an observed (expected) significance of 2.6 (2.9) standard deviations. The measurements are consistent within uncertainties with the prediction from the standard model.

Acknowledgments

We congratulate our colleagues in the CERN accelerator departments for the excellent performance of the LHC and thank the technical and administrative staffs at CERN and at other CMS institutes for their contributions to the success of the CMS effort. In addition, we gratefully acknowledge the computing centers and personnel of the Worldwide LHC Computing Grid and other centers for delivering so effectively the computing infrastructure essential to our analyses. Finally, we acknowledge the enduring support for the construction and operation of the LHC, the CMS detector, and the supporting computing infrastructure provided by the following funding agencies: SC (Armenia), BMBWF and FWF (Austria); FNRS and FWO (Belgium); CNPq, CAPES, FAPERJ, FAPERGS, and FAPESP (Brazil); MES and BNSF (Bulgaria);

CERN; CAS, MoST, and NSFC (China); MINCIENCIAS (Colombia); MSES and CSF (Croatia); RIF (Cyprus); SENESCYT (Ecuador); MoER, ERC PUT and ERDF (Estonia); Academy of Finland, MEC, and HIP (Finland); CEA and CNRS/IN2P3 (France); BMBF, DFG, and HGF (Germany); GSRI (Greece); NKFIH (Hungary); DAE and DST (India); IPM (Iran); SFI (Ireland); INFN (Italy); MSIP and NRF (Republic of Korea); MES (Latvia); LAS (Lithuania); MOE and UM (Malaysia); BUAP, CINVESTAV, CONACYT, LNS, SEP, and UASLP-FAI (Mexico); MOS (Montenegro); MBIE (New Zealand); PAEC (Pakistan); MES and NSC (Poland); FCT (Portugal); MESTD (Serbia); MCIN/AEI and PCTI (Spain); MOSTR (Sri Lanka); Swiss Funding Agencies (Switzerland); MST (Taipei); MHESI and NSTDA (Thailand); TUBITAK and TENMAK (Turkey); NASU (Ukraine); STFC (United Kingdom); DOE and NSF (USA).

Individuals have received support from the Marie-Curie program and the European Research Council and Horizon 2020 Grant, contract Nos. 675440, 724704, 752730, 758316, 765710, 824093, 884104, and COST Action CA16108 (European Union); the Leventis Foundation; the Alfred P. Sloan Foundation; the Alexander von Humboldt Foundation; the Science Committee, project no. 22rl-037 (Armenia); the Belgian Federal Science Policy Office; the Fonds pour la Formation à la Recherche dans l'Industrie et dans l'Agriculture (FRIA-Belgium); the Agentschap voor Innovatie door Wetenschap en Technologie (IWT-Belgium); the F.R.S.-FNRS and FWO (Belgium) under the "Excellence of Science – EOS" – be.h project n. 30820817; the Beijing Municipal Science & Technology Commission, No. Z191100007219010; the Ministry of Education, Youth and Sports (MEYS) of the Czech Republic; the Shota Rustaveli National Science Foundation, grant FR-22-985 (Georgia); the Deutsche Forschungsgemeinschaft (DFG), under Germany's Excellence Strategy – EXC 2121 "Quantum Universe" – 390833306, and under project number 400140256 - GRK2497; the Hellenic Foundation for Research and Innovation (HFRI), Project Number 2288 (Greece); the Hungarian Academy of Sciences, the New National Excellence Program - ÚNKP, the NKFIH research grants K 124845, K 124850, K 128713, K 128786, K 129058, K 131991, K 133046, K 138136, K 143460, K 143477, 2020-2.2.1-ED-2021-00181, and TKP2021-NKTA-64 (Hungary); the Council of Science and Industrial Research, India; the Latvian Council of Science; the Ministry of Education and Science, project no. 2022/WK/14, and the National Science Center, contracts Opus 2021/41/B/ST2/01369 and 2021/43/B/ST2/01552 (Poland); the Fundação para a Ciência e a Tecnologia, grant CEECIND/01334/2018 (Portugal); the National Priorities Research Program by Qatar National Research Fund; MCIN/AEI/10.13039/501100011033, ERDF "a way of making Europe", and the Programa Estatal de Fomento de la Investigación Científica y Técnica de Excelencia María de Maeztu, grant MDM-2017-0765 and Programa Severo Ochoa del Principado de Asturias (Spain); the Chulalongkorn Academic into Its 2nd Century Project Advancement Project, and the National Science, Research and Innovation Fund via the Program Management Unit for Human Resources & Institutional Development, Research and Innovation, grant B05F650021 (Thailand); the Kavli Foundation; the Nvidia Corporation; the SuperMicro Corporation; the Welch Foundation, contract C-1845; and the Weston Havens Foundation (USA).

References

[1] ATLAS Collaboration, "Observation of a new particle in the search for the standard model Higgs boson with the ATLAS detector at the LHC", *Phys. Lett. B* **716** (2012) 1, doi:10.1016/j.physletb.2012.08.020, arXiv:1207.7214.

[2] CMS Collaboration, "Observation of a new boson at a mass of 125 GeV with the CMS experiment at the LHC", *Phys. Lett. B* **716** (2012) 30, doi:10.1016/j.physletb.2012.08.021, arXiv:1207.7235.

[3] CMS Collaboration, "Observation of a new boson with mass near 125 GeV in pp collisions at $\sqrt{s} = 7$ and 8 TeV", *JHEP* **06** (2013) 081, doi:10.1007/JHEP06(2013)081, arXiv:1303.4571.

[4] F. Englert and R. Brout, "Broken symmetry and the mass of gauge vector mesons", *Phys. Rev. Lett.* **13** (1964) 321, doi:10.1103/PhysRevLett.13.321.

[5] P. W. Higgs, "Broken symmetries, massless particles and gauge fields", *Phys. Lett.* **12** (1964) 132, doi:10.1016/0031-9163(64)91136-9.

[6] P. W. Higgs, "Broken symmetries and the masses of gauge bosons", *Phys. Rev. Lett.* **13** (1964) 508, doi:10.1103/PhysRevLett.13.508.

[7] G. S. Guralnik, C. R. Hagen, and T. W. B. Kibble, "Global conservation laws and massless particles", *Phys. Rev. Lett.* **13** (1964) 585, doi:10.1103/PhysRevLett.13.585.

[8] P. W. Higgs, "Spontaneous symmetry breakdown without massless bosons", *Phys. Rev.* **145** (1966) 1156, doi:10.1103/PhysRev.145.1156.

[9] T. W. B. Kibble, "Symmetry breaking in non-abelian gauge theories", *Phys. Rev.* **155** (1967) 1554, doi:10.1103/PhysRev.155.1554.

[10] A. Djouadi, J. Kalinowski, and M. Spira, "HDECAY: A Program for Higgs boson decays in the standard model and its supersymmetric extension", *Comput. Phys. Commun.* **108** (1998) 56, doi:10.1016/S0010-4655(97)00123-9, arXiv:hep-ph/9704448.

[11] LHC Higgs Cross Section Working Group, "Handbook of LHC Higgs Cross Sections: 4. Deciphering the nature of the Higgs sector", *CERN Yellow Rep. Monogr.* **2** (2017) doi:10.23731/CYRM-2017-002, arXiv:1610.07922.

[12] ATLAS Collaboration, "Constraints on Higgs boson production with large transverse momentum using $H \to b\bar{b}$ decays in the ATLAS detector", *Phys. Rev. D* **105** (2022) 092003, doi:10.1103/PhysRevD.105.092003, arXiv:2111.08340.

[13] CMS Collaboration, "Inclusive search for highly boosted Higgs bosons decaying to bottom quark-antiquark pairs in proton-proton collisions at $\sqrt{s} = 13$ TeV", *JHEP* **12** (2020) 085, doi:10.1007/JHEP12(2020)085, arXiv:2006.13251.

[14] ATLAS Collaboration, "Measurements of WH and ZH production in the $H \to b\bar{b}$ decay channel in pp collisions at 13 TeV with the ATLAS detector", *Eur. Phys. J. C* **81** (2021) 178, doi:10.1140/epjc/s10052-020-08677-2, arXiv:2007.02873.

[15] CMS Collaboration, "Observation of Higgs boson decay to bottom quarks", *Phys. Rev. Lett.* **121** (2018) 121801, doi:10.1103/PhysRevLett.121.121801, arXiv:1808.08242.

[16] ATLAS Collaboration, "Measurement of Higgs boson decay into b-quarks in associated production with a top-quark pair in pp collisions at $\sqrt{s} = 13$ TeV with the ATLAS detector", *JHEP* **06** (2022) 097, doi:10.1007/JHEP06(2022)097, arXiv:2111.06712.

[17] CMS Collaboration, "Measurement of the $t\bar{t}H$ and tH production rates in the $H \to b\bar{b}$ decay channel with 138 fb^{-1} of proton-proton collision data at $\sqrt{s} = 13$ TeV", CMS Physics Analysis Summary CMS-PAS-HIG-19-011, 2023.

[18] F. Maltoni, K. Mawatari, and M. Zaro, "Higgs characterisation via vector-boson fusion and associated production: NLO and parton-shower effects", *Eur. Phys. J. C* **74** (2014) 2710, doi:10.1140/epjc/s10052-013-2710-5, arXiv:1311.1829.

[19] CMS Collaboration, "Search for the standard model Higgs boson produced through vector boson fusion and decaying to $b\bar{b}$", *Phys. Rev. D* **92** (2015) 032008, doi:10.1103/PhysRevD.92.032008, arXiv:1506.01010.

[20] ATLAS Collaboration, "Measurements of Higgs bosons decaying to bottom quarks from vector boson fusion production with the ATLAS experiment at $\sqrt{s} = 13\,\text{TeV}$", *Eur. Phys. J. C* **81** (2021) 537, doi:10.1140/epjc/s10052-021-09192-8, arXiv:2011.08280.

[21] HEPData record for this analysis, 2023. doi:10.17182/hepdata.142036.

[22] CMS Collaboration, "The CMS trigger system", *JINST* **12** (2017) P01020, doi:10.1088/1748-0221/12/01/P01020, arXiv:1609.02366.

[23] CMS Collaboration, "The CMS high level trigger", *Eur. Phys. J. C* **46** (2006) 605, doi:10.1140/epjc/s2006-02495-8, arXiv:hep-ex/0512077.

[24] CMS Collaboration, "The CMS experiment at the CERN LHC", *JINST* **3** (2008) S08004, doi:10.1088/1748-0221/3/08/S08004.

[25] CMS Collaboration, "Particle-flow reconstruction and global event description with the CMS detector", *JINST* **12** (2017) P10003, doi:10.1088/1748-0221/12/10/P10003, arXiv:1706.04965.

[26] M. Cacciari, G. P. Salam, and G. Soyez, "The anti-k_{T} jet clustering algorithm", *JHEP* **04** (2008) 063, doi:10.1088/1126-6708/2008/04/063, arXiv:0802.1189.

[27] M. Cacciari, G. P. Salam, and G. Soyez, "FastJet user manual", *Eur. Phys. J. C* **72** (2012) 1896, doi:10.1140/epjc/s10052-012-1896-2, arXiv:1111.6097.

[28] CMS Collaboration, "Jet energy scale and resolution in the CMS experiment in pp collisions at 8 TeV", *JINST* **12** (2017) P02014, doi:10.1088/1748-0221/12/02/P02014, arXiv:1607.03663.

[29] CMS Collaboration, "Identification of b-quark jets with the CMS experiment", *JINST* **8** (2013) P04013, doi:10.1088/1748-0221/8/04/P04013, arXiv:1211.4462.

[30] CMS Collaboration, "Identification of heavy-flavour jets with the CMS detector in pp collisions at 13 TeV", *JINST* **13** (2018) P05011, doi:10.1088/1748-0221/13/05/P05011, arXiv:1712.07158.

[31] E. Bols et al., "Jet flavour classification using DeepJet", *JINST* **15** (2020) P12012, doi:10.1088/1748-0221/15/12/P12012, arXiv:2008.10519.

[32] CMS Collaboration, "Performance of the DeepJet b tagging algorithm using $41.9\,\text{fb}^{-1}$ of data from proton-proton collisions at 13 TeV with Phase 1 CMS detector", CMS Detector Performance Note CMS-DP-2018-058, 2018.

[33] P. Nason, "A new method for combining NLO QCD with shower Monte Carlo algorithms", *JHEP* **11** (2004) 040, doi:10.1088/1126-6708/2004/11/040, arXiv:hep-ph/0409146.

[34] S. Frixione, P. Nason, and C. Oleari, "Matching NLO QCD computations with parton shower simulations: the POWHEG method", *JHEP* **11** (2007) 070, doi:10.1088/1126-6708/2007/11/070, arXiv:0709.2092.

[35] S. Alioli, P. Nason, C. Oleari, and E. Re, "A general framework for implementing NLO calculations in shower Monte Carlo programs: the POWHEG box", *JHEP* **06** (2010) 043, doi:10.1007/JHEP06(2010)043, arXiv:1002.2581.

[36] P. Nason and C. Oleari, "NLO Higgs boson production via vector-boson fusion matched with shower in POWHEG", *JHEP* **02** (2010) 037, doi:10.1007/JHEP02(2010)037, arXiv:0911.5299.

[37] B. Cabouat and T. Sjöstrand, "Some dipole shower studies", *Eur. Phys. J. C* **78** (2018) 226, doi:10.1140/epjc/s10052-018-5645-z, arXiv:1710.00391.

[38] T. Sjöstrand et al., "An introduction to PYTHIA8.2", *Comput. Phys. Commun.* **191** (2015) 159, doi:10.1016/j.cpc.2015.01.024, arXiv:1410.3012.

[39] J. Bellm et al., "HERWIG 7.0/HERWIG++3.0 release note", *Eur. Phys. J. C* **76** (2016) 196, doi:10.1140/epjc/s10052-016-4018-8, arXiv:1512.01178.

[40] G. Luisoni, P. Nason, C. Oleari, and F. Tramontano, "$HW^{\pm}$/HZ+0 and 1 jet at NLO with the POWHEG box interfaced to GoSam and their merging within MiNLO", *JHEP* **10** (2013) 083, doi:10.1007/JHEP10(2013)083, arXiv:1306.2542.

[41] K. Hamilton, P. Nason, C. Oleari, and G. Zanderighi, "Merging H/W/Z+0 and 1 jet at NLO with no merging scale: A path to parton shower + NNLO matching", *JHEP* **05** (2013) 082, doi:10.1007/JHEP05(2013)082, arXiv:1212.4504.

[42] E. Bagnaschi, G. Degrassi, P. Slavich, and A. Vicini, "Higgs production via gluon fusion in the POWHEG approach in the SM and in the MSSM", *JHEP* **02** (2012) 088, doi:10.1007/JHEP02(2012)088, arXiv:1111.2854.

[43] R. Frederix and S. Frixione, "Merging meets matching in MC@NLO", *JHEP* **12** (2012) 061, doi:10.1007/JHEP12(2012)061, arXiv:1209.6215.

[44] J. Alwall et al., "The automated computation of tree-level and next-to-leading order differential cross sections, and their matching to parton shower simulations", *JHEP* **07** (2014) 079, doi:10.1007/JHEP07(2014)079, arXiv:1405.0301.

[45] M. L. Mangano, M. Moretti, F. Piccinini, and M. Treccani, "Matching matrix elements and shower evolution for top-quark production in hadronic collisions", *JHEP* **01** (2007) 013, doi:10.1088/1126-6708/2007/01/013, arXiv:hep-ph/0611129.

[46] J. M. Lindert et al., "Precise predictions for V+jets dark matter backgrounds", *Eur. Phys. J. C* **77** (2017) 829, doi:10.1140/epjc/s10052-017-5389-1, arXiv:1705.04664.

[47] S. Alioli, S.-O. Moch, and P. Uwer, "Hadronic top-quark pair-production with one jet and parton showering", *JHEP* **01** (2012) 137, doi:10.1007/JHEP01(2012)137, arXiv:1110.5251.

[48] S. Alioli, P. Nason, C. Oleari, and E. Re, "NLO single-top production matched with shower in POWHEG: s- and t-channel contributions", *JHEP* **09** (2009) 111, doi:10.1088/1126-6708/2009/09/111, arXiv:0907.4076.

[49] CMS Collaboration, "Extraction and validation of a new set of CMS PYTHIA8 tunes from underlying-event measurements", *Eur. Phys. J. C* **80** (2020) 4, doi:10.1140/epjc/s10052-019-7499-4, arXiv:1903.12179.

[50] NNPDF Collaboration, "Parton distributions for the LHC Run II", *JHEP* **04** (2015) 040, doi:10.1007/JHEP04(2015)040, arXiv:1410.8849.

[51] NNPDF Collaboration, "Parton distributions from high-precision collider data", *Eur. Phys. J. C* **77** (2017) 663, doi:10.1140/epjc/s10052-017-5199-5, arXiv:1706.00428.

[52] GEANT4 Collaboration, "GEANT4—a simulation toolkit", *Nucl. Instrum. Meth. A* **506** (2003) 250, doi:10.1016/S0168-9002(03)01368-8.

[53] CMS Collaboration, "Measurement of the inclusive W and Z production cross sections in pp collisions at $\sqrt{s} = 7$ TeV", *JHEP* **10** (2011) 132, doi:10.1007/JHEP10(2011)132, arXiv:1107.4789.

[54] CMS Collaboration, "Pileup mitigation at CMS in 13 TeV data", *JINST* **15** (2020) P09018, doi:10.1088/1748-0221/15/09/P09018, arXiv:2003.00503.

[55] CMS Collaboration, "A deep neural network for simultaneous estimation of b jet energy and resolution", *Comput. Softw. Big Sci.* **4** (2020) 10, doi:10.1007/s41781-020-00041-z, arXiv:1912.06046.

[56] M. J. Oreglia, "A study of the reactions $\psi' \to \gamma\gamma\psi$". PhD thesis, Stanford University, 1980. SLAC Report SLAC-R-236.

[57] P. Speckmayer, A. Hocker, J. Stelzer, and H. Voss, "The toolkit for multivariate data analysis, TMVA 4", *J. Phys. Conf. Ser.* **219** (2010) 032057, doi:10.1088/1742-6596/219/3/032057.

[58] CMS Collaboration, "Performance of quark/gluon discrimination in 8 TeV pp data", CMS Physics Analysis Summary CMS-PAS-JME-13-002, 2013.

[59] CMS Collaboration, "Jet algorithms performance in 13 TeV data", CMS Physics Analysis Summary CMS-PAS-JME-16-003, CERN, 2017.

[60] ATLAS and CMS Collaborations, and LHC Higgs Combination Group, "Procedure for the LHC Higgs boson search combination in Summer 2011", Technical Report CMS-NOTE-2011-005, ATL-PHYS-PUB-2011-11, 2011.

[61] R. A. Fisher, "On the interpretation of χ^2 from contingency tables, and the calculation of P", *J. R. Stat. Soc.* **85** (1922) 87, doi:10.2307/2340521.

[62] CMS Collaboration, "Precision luminosity measurement in proton-proton collisions at $\sqrt{s} = 13$ TeV in 2015 and 2016 at CMS", *Eur. Phys. J. C* **81** (2021) 800, doi:10.1140/epjc/s10052-021-09538-2, arXiv:2104.01927.

[63] CMS Collaboration, "CMS luminosity measurement for the 2018 data-taking period at $\sqrt{s} = 13$ TeV", CMS Physics Analysis Summary CMS-PAS-LUM-18-002, 2019.

[64] CMS Collaboration, "Measurement of the inelastic proton-proton cross section at $\sqrt{s} = 13$ TeV", *JHEP* **07** (2018) 161, doi:10.1007/JHEP07(2018)161, arXiv:1802.02613.

[65] CMS Collaboration, "Precise determination of the mass of the Higgs boson and tests of compatibility of its couplings with the standard model predictions using proton collisions at 7 and 8 TeV", *Eur. Phys. J. C* **75** (2015) 212, doi:10.1140/epjc/s10052-015-3351-7, arXiv:1412.8662.

[66] G. Cowan, K. Cranmer, E. Gross, and O. Vitells, "Asymptotic formulae for likelihood-based tests of new physics", *Eur. Phys. J. C* **71** (2011) 1554, doi:10.1140/epjc/s10052-011-1554-0, arXiv:1007.1727. [Erratum: Eur.Phys.J.C 73, 2501 (2013)].

A The CMS Collaboration

Yerevan Physics Institute, Yerevan, Armenia
A. Hayrapetyan, A. Tumasyan[1]

Institut für Hochenergiephysik, Vienna, Austria
W. Adam, J.W. Andrejkovic, T. Bergauer, S. Chatterjee, K. Damanakis, M. Dragicevic, A. Escalante Del Valle, P.S. Hussain, M. Jeitler[2], N. Krammer, L. Lechner, D. Liko, I. Mikulec, J. Schieck[2], R. Schöfbeck, D. Schwarz, M. Sonawane, S. Templ, W. Waltenberger, C.-E. Wulz[2]

Universiteit Antwerpen, Antwerpen, Belgium
M.R. Darwish[3], T. Janssen, T. Kello[4], P. Van Mechelen

Vrije Universiteit Brussel, Brussel, Belgium
E.S. Bols, J. D'Hondt, S. Dansana, A. De Moor, M. Delcourt, H. El Faham, S. Lowette, I. Makarenko, A. Morton, D. Müller, A.R. Sahasransu, S. Tavernier, M. Tytgat[5], S. Van Putte, D. Vannerom

Université Libre de Bruxelles, Bruxelles, Belgium
B. Clerbaux, G. De Lentdecker, L. Favart, D. Hohov, J. Jaramillo, A. Khalilzadeh, K. Lee, M. Mahdavikhorrami, A. Malara, S. Paredes, L. Pétré, N. Postiau, L. Thomas, M. Vanden Bemden, C. Vander Velde, P. Vanlaer

Ghent University, Ghent, Belgium
M. De Coen, D. Dobur, J. Knolle, L. Lambrecht, G. Mestdach, C. Rendón, A. Samalan, K. Skovpen, N. Van Den Bossche, B. Vermassen, L. Wezenbeek

Université Catholique de Louvain, Louvain-la-Neuve, Belgium
A. Benecke, G. Bruno, F. Bury, C. Caputo, C. Delaere, I.S. Donertas, A. Giammanco, K. Jaffel, Sa. Jain, V. Lemaitre, J. Lidrych, P. Mastrapasqua, K. Mondal, T.T. Tran, S. Wertz

Centro Brasileiro de Pesquisas Fisicas, Rio de Janeiro, Brazil
G.A. Alves, E. Coelho, C. Hensel, A. Moraes, P. Rebello Teles

Universidade do Estado do Rio de Janeiro, Rio de Janeiro, Brazil
W.L. Aldá Júnior, M. Alves Gallo Pereira, M. Barroso Ferreira Filho, H. Brandao Malbouisson, W. Carvalho, J. Chinellato[6], E.M. Da Costa, G.G. Da Silveira[7], D. De Jesus Damiao, S. Fonseca De Souza, J. Martins[8], C. Mora Herrera, K. Mota Amarilo, L. Mundim, H. Nogima, A. Santoro, S.M. Silva Do Amaral, A. Sznajder, M. Thiel, A. Vilela Pereira

Universidade Estadual Paulista, Universidade Federal do ABC, São Paulo, Brazil
C.A. Bernardes[7], L. Calligaris, T.R. Fernandez Perez Tomei, E.M. Gregores, P.G. Mercadante, S.F. Novaes, B. Orzari, Sandra S. Padula

Institute for Nuclear Research and Nuclear Energy, Bulgarian Academy of Sciences, Sofia, Bulgaria
A. Aleksandrov, G. Antchev, R. Hadjiiska, P. Iaydjiev, M. Misheva, M. Shopova, G. Sultanov

University of Sofia, Sofia, Bulgaria
A. Dimitrov, T. Ivanov, L. Litov, B. Pavlov, P. Petkov, A. Petrov, E. Shumka

Instituto De Alta Investigación, Universidad de Tarapacá, Casilla 7 D, Arica, Chile

S. Keshri, S. Thakur

Beihang University, Beijing, China
T. Cheng, Q. Guo, T. Javaid, M. Mittal, L. Yuan

Department of Physics, Tsinghua University, Beijing, China
G. Bauer[9], Z. Hu, K. Yi[9,10]

Institute of High Energy Physics, Beijing, China
G.M. Chen[11], H.S. Chen[11], M. Chen[11], F. Iemmi, C.H. Jiang, A. Kapoor, H. Liao, Z.-A. Liu[12], F. Monti, R. Sharma, J.N. Song[12], J. Tao, J. Wang, H. Zhang

State Key Laboratory of Nuclear Physics and Technology, Peking University, Beijing, China
A. Agapitos, Y. Ban, A. Levin, C. Li, Q. Li, X. Lyu, Y. Mao, S.J. Qian, X. Sun, D. Wang, H. Yang

Sun Yat-Sen University, Guangzhou, China
M. Lu, Z. You

University of Science and Technology of China, Hefei, China
N. Lu

Institute of Modern Physics and Key Laboratory of Nuclear Physics and Ion-beam Application (MOE) - Fudan University, Shanghai, China
X. Gao[4], D. Leggat, H. Okawa, Y. Zhang

Zhejiang University, Hangzhou, Zhejiang, China
Z. Lin, C. Lu, M. Xiao

Universidad de Los Andes, Bogota, Colombia
C. Avila, D.A. Barbosa Trujillo, A. Cabrera, C. Florez, J. Fraga, J.A. Reyes Vega

Universidad de Antioquia, Medellin, Colombia
J. Mejia Guisao, F. Ramirez, M. Rodriguez, J.D. Ruiz Alvarez

University of Split, Faculty of Electrical Engineering, Mechanical Engineering and Naval Architecture, Split, Croatia
D. Giljanovic, N. Godinovic, D. Lelas, A. Sculac

University of Split, Faculty of Science, Split, Croatia
M. Kovac, T. Sculac

Institute Rudjer Boskovic, Zagreb, Croatia
P. Bargassa, V. Brigljevic, B.K. Chitroda, D. Ferencek, S. Mishra, A. Starodumov[13], T. Susa

University of Cyprus, Nicosia, Cyprus
A. Attikis, K. Christoforou, S. Konstantinou, J. Mousa, C. Nicolaou, F. Ptochos, P.A. Razis, H. Rykaczewski, H. Saka, A. Stepennov

Charles University, Prague, Czech Republic
M. Finger, M. Finger Jr., A. Kveton

Escuela Politecnica Nacional, Quito, Ecuador
E. Ayala

Universidad San Francisco de Quito, Quito, Ecuador
E. Carrera Jarrin

Academy of Scientific Research and Technology of the Arab Republic of Egypt, Egyptian Network of High Energy Physics, Cairo, Egypt
H. Abdalla[14], Y. Assran[15,16]

Center for High Energy Physics (CHEP-FU), Fayoum University, El-Fayoum, Egypt
M. Abdullah Al-Mashad, M.A. Mahmoud

National Institute of Chemical Physics and Biophysics, Tallinn, Estonia
K. Ehataht, M. Kadastik, T. Lange, S. Nandan, C. Nielsen, J. Pata, M. Raidal, L. Tani, C. Veelken

Department of Physics, University of Helsinki, Helsinki, Finland
H. Kirschenmann, K. Osterberg, M. Voutilainen

Helsinki Institute of Physics, Helsinki, Finland
S. Bharthuar, E. Brücken, F. Garcia, J. Havukainen, K.T.S. Kallonen, M.S. Kim, R. Kinnunen, T. Lampén, K. Lassila-Perini, S. Lehti, T. Lindén, M. Lotti, L. Martikainen, M. Myllymäki, M.m. Rantanen, H. Siikonen, E. Tuominen, J. Tuominiemi

Lappeenranta-Lahti University of Technology, Lappeenranta, Finland
P. Luukka, H. Petrow, T. Tuuva[†]

IRFU, CEA, Université Paris-Saclay, Gif-sur-Yvette, France
C. Amendola, M. Besancon, F. Couderc, M. Dejardin, D. Denegri, J.L. Faure, F. Ferri, S. Ganjour, P. Gras, G. Hamel de Monchenault, V. Lohezic, J. Malcles, J. Rander, A. Rosowsky, M.Ö. Sahin, A. Savoy-Navarro[17], P. Simkina, M. Titov

Laboratoire Leprince-Ringuet, CNRS/IN2P3, Ecole Polytechnique, Institut Polytechnique de Paris, Palaiseau, France
C. Baldenegro Barrera, F. Beaudette, A. Buchot Perraguin, P. Busson, A. Cappati, C. Charlot, F. Damas, O. Davignon, B. Diab, G. Falmagne, B.A. Fontana Santos Alves, S. Ghosh, R. Granier de Cassagnac, A. Hakimi, B. Harikrishnan, G. Liu, J. Motta, M. Nguyen, C. Ochando, L. Portales, R. Salerno, U. Sarkar, J.B. Sauvan, Y. Sirois, A. Tarabini, E. Vernazza, A. Zabi, A. Zghiche

Université de Strasbourg, CNRS, IPHC UMR 7178, Strasbourg, France
J.-L. Agram[18], J. Andrea, D. Apparu, D. Bloch, J.-M. Brom, E.C. Chabert, C. Collard, U. Goerlach, C. Grimault, A.-C. Le Bihan, P. Van Hove

Institut de Physique des 2 Infinis de Lyon (IP2I), Villeurbanne, France
S. Beauceron, B. Blancon, G. Boudoul, N. Chanon, J. Choi, D. Contardo, P. Depasse, C. Dozen[19], H. El Mamouni, J. Fay, S. Gascon, M. Gouzevitch, C. Greenberg, G. Grenier, B. Ille, I.B. Laktineh, M. Lethuillier, L. Mirabito, S. Perries, M. Vander Donckt, P. Verdier, J. Xiao

Georgian Technical University, Tbilisi, Georgia
A. Khvedelidze[13], I. Lomidze, Z. Tsamalaidze[13]

RWTH Aachen University, I. Physikalisches Institut, Aachen, Germany
V. Botta, L. Feld, K. Klein, M. Lipinski, D. Meuser, A. Pauls, N. Röwert, M. Teroerde

RWTH Aachen University, III. Physikalisches Institut A, Aachen, Germany
S. Diekmann, A. Dodonova, N. Eich, D. Eliseev, M. Erdmann, P. Fackeldey,

B. Fischer, T. Hebbeker, K. Hoepfner, F. Ivone, M.y. Lee, L. Mastrolorenzo, M. Merschmeyer, A. Meyer, S. Mondal, S. Mukherjee, D. Noll, A. Novak, F. Nowotny, A. Pozdnyakov, Y. Rath, W. Redjeb, F. Rehm, H. Reithler, A. Schmidt, S.C. Schuler, A. Sharma, A. Stein, F. Torres Da Silva De Araujo[20], L. Vigilante, S. Wiedenbeck, S. Zaleski

RWTH Aachen University, III. Physikalisches Institut B, Aachen, Germany
C. Dziwok, G. Flügge, W. Haj Ahmad[21], T. Kress, A. Nowack, O. Pooth, A. Stahl, T. Ziemons, A. Zotz

Deutsches Elektronen-Synchrotron, Hamburg, Germany
H. Aarup Petersen, M. Aldaya Martin, J. Alimena, S. Amoroso, Y. An, S. Baxter, M. Bayatmakou, H. Becerril Gonzalez, O. Behnke, S. Bhattacharya, F. Blekman[22], K. Borras[23], D. Brunner, A. Campbell, A. Cardini, C. Cheng, F. Colombina, S. Consuegra Rodríguez, G. Correia Silva, M. De Silva, G. Eckerlin, D. Eckstein, L.I. Estevez Banos, O. Filatov, E. Gallo[22], A. Geiser, A. Giraldi, G. Greau, V. Guglielmi, M. Guthoff, A. Jafari[24], N.Z. Jomhari, B. Kaech, M. Kasemann, H. Kaveh, C. Kleinwort, R. Kogler, M. Komm, D. Krücker, W. Lange, D. Leyva Pernia, K. Lipka[25], W. Lohmann[26], R. Mankel, I.-A. Melzer-Pellmann, M. Mendizabal Morentin, J. Metwally, A.B. Meyer, G. Milella, M. Mormile, A. Mussgiller, A. Nürnberg, Y. Otarid, D. Pérez Adán, E. Ranken, A. Raspereza, B. Ribeiro Lopes, J. Rübenach, A. Saggio, M. Scham[27,23], V. Scheurer, S. Schnake[23], P. Schütze, C. Schwanenberger[22], M. Shchedrolosiev, R.E. Sosa Ricardo, L.P. Sreelatha Pramod, D. Stafford, F. Vazzoler, A. Ventura Barroso, R. Walsh, Q. Wang, Y. Wen, K. Wichmann, L. Wiens[23], C. Wissing, S. Wuchterl, Y. Yang, A. Zimermmane Castro Santos

University of Hamburg, Hamburg, Germany
A. Albrecht, S. Albrecht, M. Antonello, S. Bein, L. Benato, M. Bonanomi, P. Connor, K. De Leo, M. Eich, K. El Morabit, Y. Fischer, A. Fröhlich, C. Garbers, E. Garutti, A. Grohsjean, M. Hajheidari, J. Haller, A. Hinzmann, H.R. Jabusch, G. Kasieczka, P. Keicher, R. Klanner, W. Korcari, T. Kramer, V. Kutzner, F. Labe, J. Lange, A. Lobanov, C. Matthies, A. Mehta, L. Moureaux, M. Mrowietz, A. Nigamova, Y. Nissan, A. Paasch, K.J. Pena Rodriguez, T. Quadfasel, B. Raciti, M. Rieger, D. Savoiu, J. Schindler, P. Schleper, M. Schröder, J. Schwandt, M. Sommerhalder, H. Stadie, G. Steinbrück, A. Tews, M. Wolf

Karlsruher Institut fuer Technologie, Karlsruhe, Germany
S. Brommer, M. Burkart, E. Butz, T. Chwalek, A. Dierlamm, A. Droll, N. Faltermann, M. Giffels, A. Gottmann, F. Hartmann[28], M. Horzela, U. Husemann, M. Klute, R. Koppenhöfer, M. Link, A. Lintuluoto, S. Maier, S. Mitra, Th. Müller, M. Neukum, M. Oh, G. Quast, K. Rabbertz, I. Shvetsov, H.J. Simonis, N. Trevisani, R. Ulrich, J. van der Linden, R.F. Von Cube, M. Wassmer, S. Wieland, R. Wolf, S. Wunsch, X. Zuo

Institute of Nuclear and Particle Physics (INPP), NCSR Demokritos, Aghia Paraskevi, Greece
G. Anagnostou, P. Assiouras, G. Daskalakis, A. Kyriakis, A. Stakia

National and Kapodistrian University of Athens, Athens, Greece
D. Karasavvas, P. Kontaxakis, G. Melachroinos, A. Panagiotou, I. Papavergou, I. Paraskevas, N. Saoulidou, K. Theofilatos, E. Tziaferi, K. Vellidis, I. Zisopoulos

National Technical University of Athens, Athens, Greece
G. Bakas, T. Chatzistavrou, G. Karapostoli, K. Kousouris, I. Papakrivopoulos, E. Siamarkou, G. Tsipolitis, A. Zacharopoulou

University of Ioánnina, Ioánnina, Greece
K. Adamidis, I. Bestintzanos, I. Evangelou, C. Foudas, P. Gianneios, C. Kamtsikis, P. Katsoulis, P. Kokkas, P.G. Kosmoglou Kioseoglou, N. Manthos, I. Papadopoulos, J. Strologas

MTA-ELTE Lendület CMS Particle and Nuclear Physics Group, Eötvös Loránd University, Budapest, Hungary
M. Csanád, K. Farkas, M.M.A. Gadallah[29], Á. Kadlecsik, P. Major, K. Mandal, G. Pásztor, A.J. Rádl[30], O. Surányi, G.I. Veres

Wigner Research Centre for Physics, Budapest, Hungary
M. Bartók[31], C. Hajdu, D. Horvath[32,33], F. Sikler, V. Veszpremi

Institute of Nuclear Research ATOMKI, Debrecen, Hungary
G. Bencze, S. Czellar, J. Karancsi[31], J. Molnar, Z. Szillasi

Institute of Physics, University of Debrecen, Debrecen, Hungary
P. Raics, B. Ujvari[34], G. Zilizi

Karoly Robert Campus, MATE Institute of Technology, Gyongyos, Hungary
T. Csorgo[30], F. Nemes[30], T. Novak

Panjab University, Chandigarh, India
J. Babbar, S. Bansal, S.B. Beri, V. Bhatnagar, G. Chaudhary, S. Chauhan, N. Dhingra[35], R. Gupta, A. Kaur, A. Kaur, H. Kaur, M. Kaur, S. Kumar, P. Kumari, M. Meena, K. Sandeep, T. Sheokand, J.B. Singh[36], A. Singla

University of Delhi, Delhi, India
A. Ahmed, A. Bhardwaj, A. Chhetri, B.C. Choudhary, A. Kumar, M. Naimuddin, K. Ranjan, S. Saumya

Saha Institute of Nuclear Physics, HBNI, Kolkata, India
S. Baradia, S. Barman[37], S. Bhattacharya, D. Bhowmik, S. Dutta, S. Dutta, B. Gomber[38], P. Palit, G. Saha, B. Sahu[38], S. Sarkar

Indian Institute of Technology Madras, Madras, India
P.K. Behera, S.C. Behera, S. Chatterjee, P. Jana, P. Kalbhor, J.R. Komaragiri[39], D. Kumar[39], M. Mohammad Mobassir Ameen, A. Muhammad, L. Panwar[39], R. Pradhan, P.R. Pujahari, N.R. Saha, A. Sharma, A.K. Sikdar, S. Verma

Tata Institute of Fundamental Research-A, Mumbai, India
T. Aziz, I. Das, S. Dugad, M. Kumar, G.B. Mohanty, P. Suryadevara

Tata Institute of Fundamental Research-B, Mumbai, India
A. Bala, S. Banerjee, M. Guchait, S. Karmakar, S. Kumar, G. Majumder, K. Mazumdar, S. Mukherjee, A. Thachayath

National Institute of Science Education and Research, An OCC of Homi Bhabha National Institute, Bhubaneswar, Odisha, India
S. Bahinipati[40], A.K. Das, C. Kar, D. Maity[41], P. Mal, T. Mishra, V.K. Muraleedharan Nair Bindhu[41], K. Naskar[41], A. Nayak[41], P. Sadangi, P. Saha, S.K. Swain, S. Varghese[41], D. Vats[41]

Indian Institute of Science Education and Research (IISER), Pune, India
A. Alpana, S. Dube, B. Kansal, A. Laha, S. Pandey, A. Rastogi, S. Sharma

Isfahan University of Technology, Isfahan, Iran
H. Bakhshiansohi[42,43], E. Khazaie[43], M. Zeinali[44]

Institute for Research in Fundamental Sciences (IPM), Tehran, Iran
S. Chenarani[45], S.M. Etesami, M. Khakzad, M. Mohammadi Najafabadi

University College Dublin, Dublin, Ireland
M. Grunewald

INFN Sezione di Bari[a], Università di Bari[b], Politecnico di Bari[c], Bari, Italy
M. Abbrescia[a,b], R. Aly[a,b,46], A. Colaleo[a], D. Creanza[a,c], B. D' Anzi[a,b], N. De Filippis[a,c], M. De Palma[a,b], A. Di Florio[a,b], W. Elmetenawee[a,b], L. Fiore[a], G. Iaselli[a,c], G. Maggi[a,c], M. Maggi[a], I. Margjeka[a,b], V. Mastrapasqua[a,b], S. My[a,b], S. Nuzzo[a,b], A. Pellecchia[a,b], A. Pompili[a,b], G. Pugliese[a,c], R. Radogna[a], D. Ramos[a], A. Ranieri[a], L. Silvestris[a], F.M. Simone[a,b], Ü. Sözbilir[a], A. Stamerra[a], R. Venditti[a], P. Verwilligen[a], A. Zaza[a,b]

INFN Sezione di Bologna[a], Università di Bologna[b], Bologna, Italy
G. Abbiendi[a], C. Battilana[a,b], D. Bonacorsi[a,b], L. Borgonovi[a], R. Campanini[a,b], P. Capiluppi[a,b], A. Castro[a,b], F.R. Cavallo[a], M. Cuffiani[a,b], G.M. Dallavalle[a], T. Diotalevi[a,b], F. Fabbri[a], A. Fanfani[a,b], D. Fasanella[a,b], P. Giacomelli[a], L. Giommi[a,b], C. Grandi[a], L. Guiducci[a,b], S. Lo Meo[a,47], L. Lunerti[a,b], S. Marcellini[a], G. Masetti[a], F.L. Navarria[a,b], F. Primavera[a,b], A.M. Rossi[a,b], T. Rovelli[a,b], G.P. Siroli[a,b]

INFN Sezione di Catania[a], Università di Catania[b], Catania, Italy
S. Costa[a,b,48], A. Di Mattia[a], R. Potenza[a,b], A. Tricomi[a,b,48], C. Tuve[a,b]

INFN Sezione di Firenze[a], Università di Firenze[b], Firenze, Italy
G. Barbagli[a], G. Bardelli[a,b], B. Camaiani[a,b], A. Cassese[a], R. Ceccarelli[a,b], V. Ciulli[a,b], C. Civinini[a], R. D'Alessandro[a,b], E. Focardi[a,b], G. Latino[a,b], P. Lenzi[a,b], M. Lizzo[a,b], M. Meschini[a], S. Paoletti[a], G. Sguazzoni[a], L. Viliani[a]

INFN Laboratori Nazionali di Frascati, Frascati, Italy
L. Benussi, S. Bianco, S. Meola[49], D. Piccolo

INFN Sezione di Genova[a], Università di Genova[b], Genova, Italy
P. Chatagnon[a], F. Ferro[a], E. Robutti[a], S. Tosi[a,b]

INFN Sezione di Milano-Bicocca[a], Università di Milano-Bicocca[b], Milano, Italy
A. Benaglia[a], G. Boldrini[a], F. Brivio[a,b], F. Cetorelli[a,b], F. De Guio[a,b], M.E. Dinardo[a,b], P. Dini[a], S. Gennai[a], A. Ghezzi[a,b], P. Govoni[a,b], L. Guzzi[a,b], M.T. Lucchini[a,b], M. Malberti[a], S. Malvezzi[a], A. Massironi[a], D. Menasce[a], L. Moroni[a], M. Paganoni[a,b], D. Pedrini[a], B.S. Pinolini[a], S. Ragazzi[a,b], N. Redaelli[a], T. Tabarelli de Fatis[a,b], D. Zuolo[a,b]

INFN Sezione di Napoli[a], Università di Napoli 'Federico II'[b], Napoli, Italy; Università della Basilicata[c], Potenza, Italy; Università G. Marconi[d], Roma, Italy
S. Buontempo[a], A. Cagnotta[a,b], F. Carnevali[a,b], N. Cavallo[a,c], A. De Iorio[a,b], F. Fabozzi[a,c], A.O.M. Iorio[a,b], L. Lista[a,b,50], P. Paolucci[a,28], B. Rossi[a], C. Sciacca[a,b]

INFN Sezione di Padova[a], Università di Padova[b], Padova, Italy; Università di Trento[c], Trento, Italy
R. Ardino[a], P. Azzi[a], N. Bacchetta[a,51], D. Bisello[a,b], P. Bortignon[a], A. Bragagnolo[a,b], R. Carlin[a,b], P. Checchia[a], T. Dorigo[a], F. Gasparini[a,b], U. Gasparini[a,b], G. Grosso[a], L. Layer[a,52], E. Lusiani[a], M. Margoni[a,b], M. Migliorini[a,b], M. Passaseo[a], J. Pazzini[a,b], P. Ronchese[a,b], R. Rossin[a,b], M. Sgaravatto[a], F. Simonetto[a,b], G. Strong[a], M. Tosi[a,b], A. Triossi[a,b], S. Ventura[a], H. Yarar[a,b], P. Zotto[a,b], A. Zucchetta[a,b], G. Zumerle[a,b]

INFN Sezione di Pavia[a], Università di Pavia[b], Pavia, Italy
S. Abu Zeid[a,53], C. Aimè[a,b], A. Braghieri[a], S. Calzaferri[a,b], D. Fiorina[a,b], P. Montagna[a,b], V. Re[a], C. Riccardi[a,b], P. Salvini[a], I. Vai[a,b], P. Vitulo[a,b]

INFN Sezione di Perugia[a], Università di Perugia[b], Perugia, Italy
S. Ajmal[a,b], P. Asenov[a,54], G.M. Bilei[a], D. Ciangottini[a,b], L. Fanò[a,b], M. Magherini[a,b], G. Mantovani[a,b], V. Mariani[a,b], M. Menichelli[a], F. Moscatelli[a,54], A. Piccinelli[a,b], M. Presilla[a,b], A. Rossi[a,b], A. Santocchia[a,b], D. Spiga[a], T. Tedeschi[a,b]

INFN Sezione di Pisa[a], Università di Pisa[b], Scuola Normale Superiore di Pisa[c], Pisa, Italy; Università di Siena[d], Siena, Italy
P. Azzurri[a], G. Bagliesi[a], R. Bhattacharya[a], L. Bianchini[a,b], T. Boccali[a], E. Bossini[a,b], D. Bruschini[a,c], R. Castaldi[a], M.A. Ciocci[a,b], V. D'Amante[a,d], R. Dell'Orso[a], S. Donato[a], A. Giassi[a], F. Ligabue[a,c], D. Matos Figueiredo[a], A. Messineo[a,b], M. Musich[a,b], F. Palla[a], S. Parolia[a], G. Ramirez-Sanchez[a,c], A. Rizzi[a,b], G. Rolandi[a,c], S. Roy Chowdhury[a], T. Sarkar[a], A. Scribano[a], P. Spagnolo[a], R. Tenchini[a], G. Tonelli[a,b], N. Turini[a,d], A. Venturi[a], P.G. Verdini[a]

INFN Sezione di Roma[a], Sapienza Università di Roma[b], Roma, Italy
P. Barria[a], M. Campana[a,b], F. Cavallari[a], L. Cunqueiro Mendez[a,b], D. Del Re[a,b], E. Di Marco[a], M. Diemoz[a], F. Errico[a,b], E. Longo[a,b], P. Meridiani[a], J. Mijuskovic[a,b], G. Organtini[a,b], F. Pandolfi[a], R. Paramatti[a,b], C. Quaranta[a,b], S. Rahatlou[a,b], C. Rovelli[a], F. Santanastasio[a,b], L. Soffi[a], R. Tramontano[a,b]

INFN Sezione di Torino[a], Università di Torino[b], Torino, Italy; Università del Piemonte Orientale[c], Novara, Italy
N. Amapane[a,b], R. Arcidiacono[a,c], S. Argiro[a,b], M. Arneodo[a,c], N. Bartosik[a], R. Bellan[a,b], A. Bellora[a,b], C. Biino[a], N. Cartiglia[a], M. Costa[a,b], R. Covarelli[a,b], N. Demaria[a], L. Finco[a], M. Grippo[a,b], B. Kiani[a,b], F. Legger[a], F. Luongo[a,b], C. Mariotti[a], S. Maselli[a], A. Mecca[a,b], E. Migliore[a,b], M. Monteno[a], R. Mulargia[a], M.M. Obertino[a,b], G. Ortona[a], L. Pacher[a,b], N. Pastrone[a], M. Pelliccioni[a], M. Ruspa[a,c], K. Shchelina[a], F. Siviero[a,b], V. Sola[a,b], A. Solano[a,b], D. Soldi[a,b], A. Staiano[a], C. Tarricone[a,b], M. Tornago[a,b], D. Trocino[a], G. Umoret[a,b], A. Vagnerini[a,b], E. Vlasov[a,b]

INFN Sezione di Trieste[a], Università di Trieste[b], Trieste, Italy
S. Belforte[a], V. Candelise[a,b], M. Casarsa[a], F. Cossutti[a], G. Della Ricca[a,b], G. Sorrentino[a,b]

Kyungpook National University, Daegu, Korea
S. Dogra, C. Huh, B. Kim, D.H. Kim, J. Kim, J. Lee, S.W. Lee, C.S. Moon, Y.D. Oh, S.I. Pak, M.S. Ryu, S. Sekmen, Y.C. Yang

Chonnam National University, Institute for Universe and Elementary Particles, Kwangju, Korea
G. Bak, P. Gwak, H. Kim, D.H. Moon

Hanyang University, Seoul, Korea
E. Asilar, D. Kim, T.J. Kim, J. Park

Korea University, Seoul, Korea
S. Choi, S. Han, B. Hong, K. Lee, K.S. Lee, J. Park, S.K. Park, J. Yoo

Kyung Hee University, Department of Physics, Seoul, Korea
J. Goh

Sejong University, Seoul, Korea
H. S. Kim, Y. Kim, S. Lee

Seoul National University, Seoul, Korea
J. Almond, J.H. Bhyun, J. Choi, S. Jeon, W. Jun, J. Kim, J.S. Kim, S. Ko, H. Kwon, H. Lee, S. Lee, B.H. Oh, S.B. Oh, H. Seo, U.K. Yang, I. Yoon

University of Seoul, Seoul, Korea
W. Jang, D.Y. Kang, Y. Kang, S. Kim, B. Ko, J.S.H. Lee, Y. Lee, J.A. Merlin, I.C. Park, Y. Roh, I.J. Watson, S. Yang

Yonsei University, Department of Physics, Seoul, Korea
S. Ha, H.D. Yoo

Sungkyunkwan University, Suwon, Korea
M. Choi, M.R. Kim, H. Lee, Y. Lee, I. Yu

College of Engineering and Technology, American University of the Middle East (AUM), Dasman, Kuwait
T. Beyrouthy, Y. Maghrbi

Riga Technical University, Riga, Latvia
K. Dreimanis, A. Gaile, G. Pikurs, A. Potrebko, M. Seidel, V. Veckalns[55]

University of Latvia (LU), Riga, Latvia
N.R. Strautnieks

Vilnius University, Vilnius, Lithuania
M. Ambrozas, A. Juodagalvis, A. Rinkevicius, G. Tamulaitis

National Centre for Particle Physics, Universiti Malaya, Kuala Lumpur, Malaysia
N. Bin Norjoharuddeen, I. Yusuff[56], Z. Zolkapli

Universidad de Sonora (UNISON), Hermosillo, Mexico
J.F. Benitez, A. Castaneda Hernandez, H.A. Encinas Acosta, L.G. Gallegos Maríñez, M. León Coello, J.A. Murillo Quijada, A. Sehrawat, L. Valencia Palomo

Centro de Investigacion y de Estudios Avanzados del IPN, Mexico City, Mexico
G. Ayala, H. Castilla-Valdez, E. De La Cruz-Burelo, I. Heredia-De La Cruz[57], R. Lopez-Fernandez, C.A. Mondragon Herrera, D.A. Perez Navarro, A. Sánchez Hernández

Universidad Iberoamericana, Mexico City, Mexico
C. Oropeza Barrera, M. Ramírez García

Benemerita Universidad Autonoma de Puebla, Puebla, Mexico
I. Bautista, I. Pedraza, H.A. Salazar Ibarguen, C. Uribe Estrada

University of Montenegro, Podgorica, Montenegro
I. Bubanja, N. Raicevic

University of Canterbury, Christchurch, New Zealand
P.H. Butler

National Centre for Physics, Quaid-I-Azam University, Islamabad, Pakistan
A. Ahmad, M.I. Asghar, A. Awais, M.I.M. Awan, H.R. Hoorani, W.A. Khan

AGH University of Science and Technology Faculty of Computer Science, Electronics and Telecommunications, Krakow, Poland
V. Avati, L. Grzanka, M. Malawski

National Centre for Nuclear Research, Swierk, Poland
H. Bialkowska, M. Bluj, B. Boimska, M. Górski, M. Kazana, M. Szleper, P. Zalewski

Institute of Experimental Physics, Faculty of Physics, University of Warsaw, Warsaw, Poland
K. Bunkowski, K. Doroba, A. Kalinowski, M. Konecki, J. Krolikowski

Laboratório de Instrumentação e Física Experimental de Partículas, Lisboa, Portugal
M. Araujo, D. Bastos, C. Beirão Da Cruz E Silva, A. Boletti, M. Bozzo, P. Faccioli, M. Gallinaro, J. Hollar, N. Leonardo, T. Niknejad, M. Pisano, J. Seixas, J. Varela

Faculty of Physics, University of Belgrade, Belgrade, Serbia
P. Adzic, P. Milenovic

VINCA Institute of Nuclear Sciences, University of Belgrade, Belgrade, Serbia
M. Dordevic, J. Milosevic, V. Rekovic

Centro de Investigaciones Energéticas Medioambientales y Tecnológicas (CIEMAT), Madrid, Spain
M. Aguilar-Benitez, J. Alcaraz Maestre, M. Barrio Luna, Cristina F. Bedoya, M. Cepeda, M. Cerrada, N. Colino, B. De La Cruz, A. Delgado Peris, D. Fernández Del Val, J.P. Fernández Ramos, J. Flix, M.C. Fouz, O. Gonzalez Lopez, S. Goy Lopez, J.M. Hernandez, M.I. Josa, J. León Holgado, D. Moran, Á. Navarro Tobar, C. Perez Dengra, A. Pérez-Calero Yzquierdo, J. Puerta Pelayo, I. Redondo, D.D. Redondo Ferrero, L. Romero, S. Sánchez Navas, L. Urda Gómez, J. Vazquez Escobar, C. Willmott

Universidad Autónoma de Madrid, Madrid, Spain
J.F. de Trocóniz

Universidad de Oviedo, Instituto Universitario de Ciencias y Tecnologías Espaciales de Asturias (ICTEA), Oviedo, Spain
B. Alvarez Gonzalez, J. Cuevas, J. Fernandez Menendez, S. Folgueras, I. Gonzalez Caballero, J.R. González Fernández, E. Palencia Cortezon, C. Ramón Álvarez, V. Rodríguez Bouza, A. Soto Rodríguez, A. Trapote, C. Vico Villalba, P. Vischia

Instituto de Física de Cantabria (IFCA), CSIC-Universidad de Cantabria, Santander, Spain
S. Bhowmik, S. Blanco Fernández, J.A. Brochero Cifuentes, I.J. Cabrillo, A. Calderon, J. Duarte Campderros, M. Fernandez, C. Fernandez Madrazo, G. Gomez, C. Lasaosa García, C. Martinez Rivero, P. Martinez Ruiz del Arbol,

F. Matorras, P. Matorras Cuevas, E. Navarrete Ramos, J. Piedra Gomez, C. Prieels, L. Scodellaro, I. Vila, J.M. Vizan Garcia

University of Colombo, Colombo, Sri Lanka
M.K. Jayananda, B. Kailasapathy[58], D.U.J. Sonnadara, D.D.C. Wickramarathna

University of Ruhuna, Department of Physics, Matara, Sri Lanka
W.G.D. Dharmaratna, K. Liyanage, N. Perera, N. Wickramage

CERN, European Organization for Nuclear Research, Geneva, Switzerland
D. Abbaneo, E. Auffray, G. Auzinger, J. Baechler, D. Barney, A. Bermúdez Martínez, M. Bianco, B. Bilin, A.A. Bin Anuar, A. Bocci, E. Brondolin, C. Caillol, T. Camporesi, G. Cerminara, N. Chernyavskaya, M. Cipriani, D. d'Enterria, A. Dabrowski, A. David, A. De Roeck, M.M. Defranchis, M. Deile, M. Dobson, F. Fallavollita[59], L. Forthomme, G. Franzoni, W. Funk, S. Giani, D. Gigi, K. Gill, F. Glege, L. Gouskos, M. Haranko, J. Hegeman, T. James, J. Kieseler, N. Kratochwil, S. Laurila, P. Lecoq, E. Leutgeb, C. Lourenço, B. Maier, L. Malgeri, M. Mannelli, A.C. Marini, F. Meijers, S. Mersi, E. Meschi, V. Milosevic, F. Moortgat, M. Mulders, S. Orfanelli, F. Pantaleo, M. Peruzzi, A. Petrilli, G. Petrucciani, A. Pfeiffer, M. Pierini, D. Piparo, H. Qu, D. Rabady, G. Reales Gutiérrez, M. Rovere, H. Sakulin, S. Scarfi, M. Selvaggi, A. Sharma, P. Silva, P. Sphicas[60], A.G. Stahl Leiton, A. Steen, S. Summers, D. Treille, P. Tropea, A. Tsirou, D. Walter, J. Wanczyk[61], K.A. Wozniak, P. Zehetner, P. Zejdl, W.D. Zeuner

Paul Scherrer Institut, Villigen, Switzerland
T. Bevilacqua[62], L. Caminada[62], A. Ebrahimi, W. Erdmann, R. Horisberger, Q. Ingram, H.C. Kaestli, D. Kotlinski, C. Lange, M. Missiroli[62], L. Noehte[62], T. Rohe

ETH Zurich - Institute for Particle Physics and Astrophysics (IPA), Zurich, Switzerland
T.K. Aarrestad, K. Androsov[61], M. Backhaus, A. Calandri, K. Datta, A. De Cosa, G. Dissertori, M. Dittmar, M. Donegà, F. Eble, M. Galli, K. Gedia, F. Glessgen, C. Grab, D. Hits, W. Lustermann, A.-M. Lyon, R.A. Manzoni, L. Marchese, C. Martin Perez, A. Mascellani[61], F. Nessi-Tedaldi, F. Pauss, V. Perovic, S. Pigazzini, M.G. Ratti, M. Reichmann, C. Reissel, T. Reitenspiess, B. Ristic, F. Riti, D. Ruini, D.A. Sanz Becerra, R. Seidita, J. Steggemann[61], D. Valsecchi, R. Wallny

Universität Zürich, Zurich, Switzerland
C. Amsler[63], P. Bärtschi, C. Botta, D. Brzhechko, M.F. Canelli, K. Cormier, A. De Wit, R. Del Burgo, J.K. Heikkilä, M. Huwiler, W. Jin, A. Jofrehei, B. Kilminster, S. Leontsinis, S.P. Liechti, A. Macchiolo, P. Meiring, V.M. Mikuni, U. Molinatti, I. Neutelings, A. Reimers, P. Robmann, S. Sanchez Cruz, K. Schweiger, M. Senger, Y. Takahashi

National Central University, Chung-Li, Taiwan
C. Adloff[64], C.M. Kuo, W. Lin, P.K. Rout, P.C. Tiwari[39], S.S. Yu

National Taiwan University (NTU), Taipei, Taiwan
L. Ceard, Y. Chao, K.F. Chen, P.s. Chen, W.-S. Hou, Y.w. Kao, R. Khurana, G. Kole, Y.y. Li, R.-S. Lu, E. Paganis, A. Psallidas, J. Thomas-Wilsker, H.y. Wu, E. Yazgan

Chulalongkorn University, Faculty of Science, Department of Physics, Bangkok, Thailand

C. Asawatangtrakuldee, N. Srimanobhas, V. Wachirapusitanand

Çukurova University, Physics Department, Science and Art Faculty, Adana, Turkey
D. Agyel, F. Boran, Z.S. Demiroglu, F. Dolek, I. Dumanoglu[65], E. Eskut, Y. Guler[66], E. Gurpinar Guler[66], C. Isik, O. Kara, A. Kayis Topaksu, U. Kiminsu, G. Onengut, K. Ozdemir[67], A. Polatoz, B. Tali[68], U.G. Tok, S. Turkcapar, E. Uslan, I.S. Zorbakir

Middle East Technical University, Physics Department, Ankara, Turkey
K. Ocalan[69], M. Yalvac[70]

Bogazici University, Istanbul, Turkey
B. Akgun, I.O. Atakisi, E. Gülmez, M. Kaya[71], O. Kaya[72], S. Tekten[73]

Istanbul Technical University, Istanbul, Turkey
A. Cakir, K. Cankocak[65], Y. Komurcu, S. Sen[74]

Istanbul University, Istanbul, Turkey
O. Aydilek, S. Cerci[68], V. Epshteyn, B. Hacisahinoglu, I. Hos[75], B. Isildak[76], B. Kaynak, S. Ozkorucuklu, H. Sert, C. Simsek, D. Sunar Cerci[68], C. Zorbilmez

Institute for Scintillation Materials of National Academy of Science of Ukraine, Kharkiv, Ukraine
A. Boyaryntsev, B. Grynyov

National Science Centre, Kharkiv Institute of Physics and Technology, Kharkiv, Ukraine
L. Levchuk

University of Bristol, Bristol, United Kingdom
D. Anthony, J.J. Brooke, A. Bundock, E. Clement, D. Cussans, H. Flacher, M. Glowacki, J. Goldstein, H.F. Heath, L. Kreczko, B. Krikler, S. Paramesvaran, S. Seif El Nasr-Storey, V.J. Smith, N. Stylianou[77], K. Walkingshaw Pass, R. White

Rutherford Appleton Laboratory, Didcot, United Kingdom
A.H. Ball, K.W. Bell, A. Belyaev[78], C. Brew, R.M. Brown, D.J.A. Cockerill, C. Cooke, K.V. Ellis, K. Harder, S. Harper, M.-L. Holmberg[79], Sh. Jain, J. Linacre, K. Manolopoulos, D.M. Newbold, E. Olaiya, D. Petyt, T. Reis, G. Salvi, T. Schuh, C.H. Shepherd-Themistocleous, I.R. Tomalin, T. Williams

Imperial College, London, United Kingdom
R. Bainbridge, P. Bloch, C.E. Brown, O. Buchmuller, V. Cacchio, C.A. Carrillo Montoya, V. Cepaitis, G.S. Chahal[80], D. Colling, J.S. Dancu, P. Dauncey, G. Davies, J. Davies, M. Della Negra, S. Fayer, G. Fedi, G. Hall, M.H. Hassanshahi, A. Howard, G. Iles, J. Langford, L. Lyons, A.-M. Magnan, S. Malik, A. Martelli, M. Mieskolainen, J. Nash[81], M. Pesaresi, B.C. Radburn-Smith, A. Richards, A. Rose, C. Seez, R. Shukla, A. Tapper, K. Uchida, G.P. Uttley, L.H. Vage, T. Virdee[28], M. Vojinovic, N. Wardle, D. Winterbottom

Brunel University, Uxbridge, United Kingdom
K. Coldham, J.E. Cole, A. Khan, P. Kyberd, I.D. Reid

Baylor University, Waco, Texas, USA
S. Abdullin, A. Brinkerhoff, B. Caraway, J. Dittmann, K. Hatakeyama, J. Hiltbrand, A.R. Kanuganti, B. McMaster, M. Saunders, S. Sawant, C. Sutantawibul, M. Toms, J. Wilson

Catholic University of America, Washington, DC, USA
R. Bartek, A. Dominguez, C. Huerta Escamilla, A.E. Simsek, R. Uniyal, A.M. Vargas Hernandez

The University of Alabama, Tuscaloosa, Alabama, USA
R. Chudasama, S.I. Cooper, S.V. Gleyzer, C.U. Perez, P. Rumerio[82], E. Usai, C. West

Boston University, Boston, Massachusetts, USA
A. Akpinar, A. Albert, D. Arcaro, C. Cosby, Z. Demiragli, C. Erice, E. Fontanesi, D. Gastler, J. Rohlf, K. Salyer, D. Sperka, D. Spitzbart, I. Suarez, A. Tsatsos, S. Yuan

Brown University, Providence, Rhode Island, USA
G. Benelli, X. Coubez[23], D. Cutts, M. Hadley, U. Heintz, J.M. Hogan[83], T. Kwon, G. Landsberg, K.T. Lau, D. Li, J. Luo, M. Narain, N. Pervan, S. Sagir[84], F. Simpson, W.Y. Wong, X. Yan, D. Yu, W. Zhang

University of California, Davis, Davis, California, USA
S. Abbott, J. Bonilla, C. Brainerd, R. Breedon, M. Calderon De La Barca Sanchez, M. Chertok, M. Citron, J. Conway, P.T. Cox, R. Erbacher, G. Haza, F. Jensen, O. Kukral, G. Mocellin, M. Mulhearn, D. Pellett, B. Regnery, W. Wei, Y. Yao, F. Zhang

University of California, Los Angeles, California, USA
M. Bachtis, R. Cousins, A. Datta, J. Hauser, M. Ignatenko, M.A. Iqbal, T. Lam, E. Manca, W.A. Nash, D. Saltzberg, B. Stone, V. Valuev

University of California, Riverside, Riverside, California, USA
R. Clare, M. Gordon, G. Hanson, W. Si, S. Wimpenny[†]

University of California, San Diego, La Jolla, California, USA
J.G. Branson, S. Cittolin, S. Cooperstein, D. Diaz, J. Duarte, R. Gerosa, L. Giannini, J. Guiang, R. Kansal, V. Krutelyov, R. Lee, J. Letts, M. Masciovecchio, F. Mokhtar, M. Pieri, M. Quinnan, B.V. Sathia Narayanan, V. Sharma, M. Tadel, E. Vourliotis, F. Würthwein, Y. Xiang, A. Yagil

University of California, Santa Barbara - Department of Physics, Santa Barbara, California, USA
L. Brennan, C. Campagnari, G. Collura, A. Dorsett, J. Incandela, M. Kilpatrick, J. Kim, A.J. Li, P. Masterson, H. Mei, M. Oshiro, J. Richman, U. Sarica, R. Schmitz, F. Setti, J. Sheplock, D. Stuart, S. Wang

California Institute of Technology, Pasadena, California, USA
A. Bornheim, O. Cerri, A. Latorre, J.M. Lawhorn, J. Mao, H.B. Newman, T. Q. Nguyen, M. Spiropulu, J.R. Vlimant, C. Wang, S. Xie, R.Y. Zhu

Carnegie Mellon University, Pittsburgh, Pennsylvania, USA
J. Alison, S. An, M.B. Andrews, P. Bryant, V. Dutta, T. Ferguson, A. Harilal, C. Liu, T. Mudholkar, S. Murthy, M. Paulini, A. Roberts, A. Sanchez, W. Terrill

University of Colorado Boulder, Boulder, Colorado, USA
J.P. Cumalat, W.T. Ford, A. Hassani, G. Karathanasis, E. MacDonald, N. Manganelli, F. Marini, A. Perloff, C. Savard, N. Schonbeck, K. Stenson, K.A. Ulmer, S.R. Wagner, N. Zipper

Cornell University, Ithaca, New York, USA
J. Alexander, S. Bright-Thonney, X. Chen, D.J. Cranshaw, J. Fan, X. Fan, D. Gadkari, S. Hogan, J. Monroy, J.R. Patterson, J. Reichert, M. Reid, A. Ryd, J. Thom, P. Wittich, R. Zou

Fermi National Accelerator Laboratory, Batavia, Illinois, USA
M. Albrow, M. Alyari, O. Amram, G. Apollinari, A. Apresyan, L.A.T. Bauerdick, D. Berry, J. Berryhill, P.C. Bhat, K. Burkett, J.N. Butler, A. Canepa, G.B. Cerati, H.W.K. Cheung, F. Chlebana, G. Cummings, J. Dickinson, I. Dutta, V.D. Elvira, Y. Feng, J. Freeman, A. Gandrakota, Z. Gecse, L. Gray, D. Green, S. Grünendahl, D. Guerrero, O. Gutsche, R.M. Harris, R. Heller, T.C. Herwig, J. Hirschauer, L. Horyn, B. Jayatilaka, S. Jindariani, M. Johnson, U. Joshi, T. Klijnsma, B. Klima, K.H.M. Kwok, S. Lammel, D. Lincoln, R. Lipton, T. Liu, C. Madrid, K. Maeshima, C. Mantilla, D. Mason, P. McBride, P. Merkel, S. Mrenna, S. Nahn, J. Ngadiuba, D. Noonan, V. Papadimitriou, N. Pastika, K. Pedro, C. Pena[85], F. Ravera, A. Reinsvold Hall[86], L. Ristori, E. Sexton-Kennedy, N. Smith, A. Soha, L. Spiegel, S. Stoynev, L. Taylor, S. Tkaczyk, N.V. Tran, L. Uplegger, E.W. Vaandering, I. Zoi

University of Florida, Gainesville, Florida, USA
C. Aruta, P. Avery, D. Bourilkov, L. Cadamuro, P. Chang, V. Cherepanov, R.D. Field, E. Koenig, M. Kolosova, J. Konigsberg, A. Korytov, K.H. Lo, K. Matchev, N. Menendez, G. Mitselmakher, A. Muthirakalayil Madhu, N. Rawal, D. Rosenzweig, S. Rosenzweig, K. Shi, J. Wang

Florida State University, Tallahassee, Florida, USA
T. Adams, A. Al Kadhim, A. Askew, N. Bower, R. Habibullah, V. Hagopian, R. Hashmi, R.S. Kim, S. Kim, T. Kolberg, G. Martinez, H. Prosper, P.R. Prova, O. Viazlo, M. Wulansatiti, R. Yohay, J. Zhang

Florida Institute of Technology, Melbourne, Florida, USA
B. Alsufyani, M.M. Baarmand, S. Butalla, T. Elkafrawy[53], M. Hohlmann, R. Kumar Verma, M. Rahmani, F. Yumiceva

University of Illinois at Chicago (UIC), Chicago, Illinois, USA
M.R. Adams, C. Bennett, R. Cavanaugh, S. Dittmer, O. Evdokimov, C.E. Gerber, D.J. Hofman, J.h. Lee, D. S. Lemos, A.H. Merrit, C. Mills, S. Nanda, G. Oh, D. Pilipovic, T. Roy, S. Rudrabhatla, M.B. Tonjes, N. Varelas, X. Wang, Z. Ye, J. Yoo

The University of Iowa, Iowa City, Iowa, USA
M. Alhusseini, D. Blend, K. Dilsiz[87], L. Emediato, G. Karaman, O.K. Köseyan, J.-P. Merlo, A. Mestvirishvili[88], J. Nachtman, O. Neogi, H. Ogul[89], Y. Onel, A. Penzo, C. Snyder, E. Tiras[90]

Johns Hopkins University, Baltimore, Maryland, USA
B. Blumenfeld, L. Corcodilos, J. Davis, A.V. Gritsan, L. Kang, S. Kyriacou, P. Maksimovic, M. Roguljic, J. Roskes, S. Sekhar, M. Swartz, T.Á. Vámi

The University of Kansas, Lawrence, Kansas, USA
A. Abreu, L.F. Alcerro Alcerro, J. Anguiano, P. Baringer, A. Bean, Z. Flowers, J. King, G. Krintiras, M. Lazarovits, C. Le Mahieu, C. Lindsey, J. Marquez, N. Minafra, M. Murray, M. Nickel, M. Pitt, S. Popescu[91], C. Rogan, C. Royon,

R. Salvatico, S. Sanders, C. Smith, Q. Wang, G. Wilson

Kansas State University, Manhattan, Kansas, USA
B. Allmond, A. Ivanov, K. Kaadze, A. Kalogeropoulos, D. Kim, Y. Maravin, K. Nam, J. Natoli, D. Roy

Lawrence Livermore National Laboratory, Livermore, California, USA
F. Rebassoo, D. Wright

University of Maryland, College Park, Maryland, USA
E. Adams, A. Baden, O. Baron, A. Belloni, A. Bethani, Y.m. Chen, S.C. Eno, N.J. Hadley, S. Jabeen, R.G. Kellogg, T. Koeth, Y. Lai, S. Lascio, A.C. Mignerey, S. Nabili, C. Palmer, C. Papageorgakis, L. Wang, K. Wong

Massachusetts Institute of Technology, Cambridge, Massachusetts, USA
J. Bendavid, W. Busza, I.A. Cali, Y. Chen, M. D'Alfonso, J. Eysermans, C. Freer, G. Gomez-Ceballos, M. Goncharov, P. Harris, D. Hoang, D. Kovalskyi, J. Krupa, L. Lavezzo, Y.-J. Lee, K. Long, C. Mironov, C. Paus, D. Rankin, C. Roland, G. Roland, S. Rothman, Z. Shi, G.S.F. Stephans, J. Wang, Z. Wang, B. Wyslouch, T. J. Yang

University of Minnesota, Minneapolis, Minnesota, USA
R.M. Chatterjee, B. Crossman, B.M. Joshi, C. Kapsiak, M. Krohn, D. Mahon, J. Mans, M. Revering, R. Rusack, R. Saradhy, N. Schroeder, N. Strobbe, M.A. Wadud

University of Mississippi, Oxford, Mississippi, USA
L.M. Cremaldi

University of Nebraska-Lincoln, Lincoln, Nebraska, USA
K. Bloom, M. Bryson, D.R. Claes, C. Fangmeier, F. Golf, C. Joo, I. Kravchenko, I. Reed, J.E. Siado, G.R. Snow[†], W. Tabb, A. Wightman, F. Yan, A.G. Zecchinelli

State University of New York at Buffalo, Buffalo, New York, USA
G. Agarwal, H. Bandyopadhyay, L. Hay, I. Iashvili, A. Kharchilava, C. McLean, M. Morris, D. Nguyen, J. Pekkanen, S. Rappoccio, H. Rejeb Sfar, A. Williams

Northeastern University, Boston, Massachusetts, USA
G. Alverson, E. Barberis, Y. Haddad, Y. Han, A. Krishna, J. Li, G. Madigan, B. Marzocchi, D.M. Morse, V. Nguyen, T. Orimoto, A. Parker, L. Skinnari, A. Tishelman-Charny, B. Wang, D. Wood

Northwestern University, Evanston, Illinois, USA
S. Bhattacharya, J. Bueghly, Z. Chen, A. Gilbert, K.A. Hahn, Y. Liu, D.G. Monk, M.H. Schmitt, A. Taliercio, M. Velasco

University of Notre Dame, Notre Dame, Indiana, USA
R. Band, R. Bucci, S. Castells, M. Cremonesi, A. Das, R. Goldouzian, M. Hildreth, K.W. Ho, K. Hurtado Anampa, C. Jessop, K. Lannon, J. Lawrence, N. Loukas, L. Lutton, J. Mariano, N. Marinelli, I. Mcalister, T. McCauley, C. Mcgrady, K. Mohrman, C. Moore, Y. Musienko[13], H. Nelson, R. Ruchti, A. Townsend, M. Wayne, H. Yockey, M. Zarucki, L. Zygala

The Ohio State University, Columbus, Ohio, USA
B. Bylsma, M. Carrigan, L.S. Durkin, C. Hill, M. Joyce, A. Lesauvage,

M. Nunez Ornelas, K. Wei, B.L. Winer, B. R. Yates

Princeton University, Princeton, New Jersey, USA
F.M. Addesa, H. Bouchamaoui, P. Das, G. Dezoort, P. Elmer, A. Frankenthal, B. Greenberg, N. Haubrich, S. Higginbotham, G. Kopp, S. Kwan, D. Lange, A. Loeliger, D. Marlow, I. Ojalvo, J. Olsen, D. Stickland, C. Tully

University of Puerto Rico, Mayaguez, Puerto Rico, USA
S. Malik

Purdue University, West Lafayette, Indiana, USA
A.S. Bakshi, V.E. Barnes, S. Chandra, R. Chawla, S. Das, A. Gu, L. Gutay, M. Jones, A.W. Jung, D. Kondratyev, A.M. Koshy, M. Liu, G. Negro, N. Neumeister, G. Paspalaki, S. Piperov, A. Purohit, J.F. Schulte, M. Stojanovic[17], J. Thieman, A. K. Virdi, F. Wang, W. Xie

Purdue University Northwest, Hammond, Indiana, USA
J. Dolen, N. Parashar, A. Pathak

Rice University, Houston, Texas, USA
D. Acosta, A. Baty, T. Carnahan, S. Dildick, K.M. Ecklund, P.J. Fernández Manteca, S. Freed, P. Gardner, F.J.M. Geurts, A. Kumar, W. Li, O. Miguel Colin, B.P. Padley, R. Redjimi, J. Rotter, S. Yang, E. Yigitbasi, Y. Zhang

University of Rochester, Rochester, New York, USA
A. Bodek, P. de Barbaro, R. Demina, J.L. Dulemba, C. Fallon, A. Garcia-Bellido, O. Hindrichs, A. Khukhunaishvili, P. Parygin, E. Popova, R. Taus, G.P. Van Onsem

The Rockefeller University, New York, New York, USA
K. Goulianos

Rutgers, The State University of New Jersey, Piscataway, New Jersey, USA
B. Chiarito, J.P. Chou, Y. Gershtein, E. Halkiadakis, A. Hart, M. Heindl, D. Jaroslawski, O. Karacheban[26], I. Laflotte, A. Lath, R. Montalvo, K. Nash, M. Osherson, H. Routray, S. Salur, S. Schnetzer, S. Somalwar, R. Stone, S.A. Thayil, S. Thomas, J. Vora, H. Wang

University of Tennessee, Knoxville, Tennessee, USA
H. Acharya, A.G. Delannoy, S. Fiorendi, T. Holmes, N. Karunarathna, L. Lee, E. Nibigira, S. Spanier

Texas A&M University, College Station, Texas, USA
M. Ahmad, O. Bouhali[92], M. Dalchenko, R. Eusebi, J. Gilmore, T. Huang, T. Kamon[93], H. Kim, S. Luo, S. Malhotra, R. Mueller, D. Overton, D. Rathjens, A. Safonov

Texas Tech University, Lubbock, Texas, USA
N. Akchurin, J. Damgov, V. Hegde, A. Hussain, Y. Kazhykarim, K. Lamichhane, S.W. Lee, A. Mankel, T. Mengke, S. Muthumuni, T. Peltola, I. Volobouev, A. Whitbeck

Vanderbilt University, Nashville, Tennessee, USA
E. Appelt, S. Greene, A. Gurrola, W. Johns, R. Kunnawalkam Elayavalli, A. Melo, F. Romeo, P. Sheldon, S. Tuo, J. Velkovska, J. Viinikainen

University of Virginia, Charlottesville, Virginia, USA
B. Cardwell, B. Cox, J. Hakala, R. Hirosky, A. Ledovskoy, A. Li, C. Neu, C.E. Perez Lara

Wayne State University, Detroit, Michigan, USA
P.E. Karchin

University of Wisconsin - Madison, Madison, Wisconsin, USA
A. Aravind, S. Banerjee, K. Black, T. Bose, S. Dasu, I. De Bruyn, P. Everaerts, C. Galloni, H. He, M. Herndon, A. Herve, C.K. Koraka, A. Lanaro, R. Loveless, J. Madhusudanan Sreekala, A. Mallampalli, A. Mohammadi, S. Mondal, G. Parida, D. Pinna, A. Savin, V. Shang, V. Sharma, W.H. Smith, D. Teague, H.F. Tsoi, W. Vetens, A. Warden

Authors affiliated with an institute or an international laboratory covered by a cooperation agreement with CERN
S. Afanasiev, V. Andreev, Yu. Andreev, T. Aushev, M. Azarkin, A. Babaev, A. Belyaev, V. Blinov[94], E. Boos, V. Borshch, D. Budkouski, V. Bunichev, V. Chekhovsky, R. Chistov[94], M. Danilov[94], A. Dermenev, T. Dimova[94], D. Druzhkin[95], M. Dubinin[85], L. Dudko, A. Ershov, G. Gavrilov, V. Gavrilov, S. Gninenko, V. Golovtcov, N. Golubev, I. Golutvin, I. Gorbunov, A. Gribushin, Y. Ivanov, V. Kachanov, L. Kardapoltsev[94], V. Karjavine, A. Karneyeu, V. Kim[94], M. Kirakosyan, D. Kirpichnikov, M. Kirsanov, V. Klyukhin, O. Kodolova[96], D. Konstantinov, V. Korenkov, A. Kozyrev[94], N. Krasnikov, A. Lanev, P. Levchenko[97], N. Lychkovskaya, V. Makarenko, A. Malakhov, V. Matveev[94], V. Murzin, A. Nikitenko[98,96], S. Obraztsov, V. Oreshkin, A. Oskin, V. Palichik, V. Perelygin, M. Perfilov, S. Polikarpov[94], V. Popov, O. Radchenko[94], M. Savina, V. Savrin, D. Selivanova, V. Shalaev, S. Shmatov, S. Shulha, Y. Skovpen[94], S. Slabospitskii, V. Smirnov, D. Sosnov, V. Sulimov, E. Tcherniaev, A. Terkulov, O. Teryaev, I. Tlisova, A. Toropin, L. Uvarov, A. Uzunian, A. Vorobyev†, N. Voytishin, B.S. Yuldashev[99], A. Zarubin, I. Zhizhin, A. Zhokin

†: Deceased
[1]Also at Yerevan State University, Yerevan, Armenia
[2]Also at TU Wien, Vienna, Austria
[3]Also at Institute of Basic and Applied Sciences, Faculty of Engineering, Arab Academy for Science, Technology and Maritime Transport, Alexandria, Egypt
[4]Also at Université Libre de Bruxelles, Bruxelles, Belgium
[5]Also at Ghent University, Ghent, Belgium
[6]Also at Universidade Estadual de Campinas, Campinas, Brazil
[7]Also at Federal University of Rio Grande do Sul, Porto Alegre, Brazil
[8]Also at UFMS, Nova Andradina, Brazil
[9]Also at Nanjing Normal University, Nanjing, China
[10]Now at The University of Iowa, Iowa City, Iowa, USA
[11]Also at University of Chinese Academy of Sciences, Beijing, China
[12]Also at University of Chinese Academy of Sciences, Beijing, China
[13]Also at an institute or an international laboratory covered by a cooperation agreement with CERN
[14]Also at Cairo University, Cairo, Egypt
[15]Also at Suez University, Suez, Egypt
[16]Now at British University in Egypt, Cairo, Egypt

[17]Also at Purdue University, West Lafayette, Indiana, USA
[18]Also at Université de Haute Alsace, Mulhouse, France
[19]Also at Department of Physics, Tsinghua University, Beijing, China
[20]Also at The University of the State of Amazonas, Manaus, Brazil
[21]Also at Erzincan Binali Yildirim University, Erzincan, Turkey
[22]Also at University of Hamburg, Hamburg, Germany
[23]Also at RWTH Aachen University, III. Physikalisches Institut A, Aachen, Germany
[24]Also at Isfahan University of Technology, Isfahan, Iran
[25]Also at Bergische University Wuppertal (BUW), Wuppertal, Germany
[26]Also at Brandenburg University of Technology, Cottbus, Germany
[27]Also at Forschungszentrum Jülich, Juelich, Germany
[28]Also at CERN, European Organization for Nuclear Research, Geneva, Switzerland
[29]Also at Physics Department, Faculty of Science, Assiut University, Assiut, Egypt
[30]Also at Wigner Research Centre for Physics, Budapest, Hungary
[31]Also at Institute of Physics, University of Debrecen, Debrecen, Hungary
[32]Also at Institute of Nuclear Research ATOMKI, Debrecen, Hungary
[33]Now at Universitatea Babes-Bolyai - Facultatea de Fizica, Cluj-Napoca, Romania
[34]Also at Faculty of Informatics, University of Debrecen, Debrecen, Hungary
[35]Also at Punjab Agricultural University, Ludhiana, India
[36]Also at UPES - University of Petroleum and Energy Studies, Dehradun, India
[37]Also at University of Visva-Bharati, Santiniketan, India
[38]Also at University of Hyderabad, Hyderabad, India
[39]Also at Indian Institute of Science (IISc), Bangalore, India
[40]Also at IIT Bhubaneswar, Bhubaneswar, India
[41]Also at Institute of Physics, Bhubaneswar, India
[42]Also at Deutsches Elektronen-Synchrotron, Hamburg, Germany
[43]Now at Department of Physics, Isfahan University of Technology, Isfahan, Iran
[44]Also at Sharif University of Technology, Tehran, Iran
[45]Also at Department of Physics, University of Science and Technology of Mazandaran, Behshahr, Iran
[46]Also at Helwan University, Cairo, Egypt
[47]Also at Italian National Agency for New Technologies, Energy and Sustainable Economic Development, Bologna, Italy
[48]Also at Centro Siciliano di Fisica Nucleare e di Struttura Della Materia, Catania, Italy
[49]Also at Università degli Studi Guglielmo Marconi, Roma, Italy
[50]Also at Scuola Superiore Meridionale, Università di Napoli 'Federico II', Napoli, Italy
[51]Also at Fermi National Accelerator Laboratory, Batavia, Illinois, USA
[52]Also at Università di Napoli 'Federico II', Napoli, Italy
[53]Also at Ain Shams University, Cairo, Egypt
[54]Also at Consiglio Nazionale delle Ricerche - Istituto Officina dei Materiali, Perugia, Italy
[55]Also at Riga Technical University, Riga, Latvia
[56]Also at Department of Applied Physics, Faculty of Science and Technology, Universiti Kebangsaan Malaysia, Bangi, Malaysia
[57]Also at Consejo Nacional de Ciencia y Tecnología, Mexico City, Mexico
[58]Also at Trincomalee Campus, Eastern University, Sri Lanka, Nilaveli, Sri Lanka
[59]Also at INFN Sezione di Pavia, Università di Pavia, Pavia, Italy
[60]Also at National and Kapodistrian University of Athens, Athens, Greece
[61]Also at Ecole Polytechnique Fédérale Lausanne, Lausanne, Switzerland
[62]Also at Universität Zürich, Zurich, Switzerland

[63]Also at Stefan Meyer Institute for Subatomic Physics, Vienna, Austria
[64]Also at Laboratoire d'Annecy-le-Vieux de Physique des Particules, IN2P3-CNRS, Annecy-le-Vieux, France
[65]Also at Near East University, Research Center of Experimental Health Science, Mersin, Turkey
[66]Also at Konya Technical University, Konya, Turkey
[67]Also at Izmir Bakircay University, Izmir, Turkey
[68]Also at Adiyaman University, Adiyaman, Turkey
[69]Also at Necmettin Erbakan University, Konya, Turkey
[70]Also at Bozok Universitetesi Rektörlügü, Yozgat, Turkey
[71]Also at Marmara University, Istanbul, Turkey
[72]Also at Milli Savunma University, Istanbul, Turkey
[73]Also at Kafkas University, Kars, Turkey
[74]Also at Hacettepe University, Ankara, Turkey
[75]Also at Istanbul University - Cerrahpasa, Faculty of Engineering, Istanbul, Turkey
[76]Also at Yildiz Technical University, Istanbul, Turkey
[77]Also at Vrije Universiteit Brussel, Brussel, Belgium
[78]Also at School of Physics and Astronomy, University of Southampton, Southampton, United Kingdom
[79]Also at University of Bristol, Bristol, United Kingdom
[80]Also at IPPP Durham University, Durham, United Kingdom
[81]Also at Monash University, Faculty of Science, Clayton, Australia
[82]Also at Università di Torino, Torino, Italy
[83]Also at Bethel University, St. Paul, Minnesota, USA
[84]Also at Karamanoğlu Mehmetbey University, Karaman, Turkey
[85]Also at California Institute of Technology, Pasadena, California, USA
[86]Also at United States Naval Academy, Annapolis, Maryland, USA
[87]Also at Bingol University, Bingol, Turkey
[88]Also at Georgian Technical University, Tbilisi, Georgia
[89]Also at Sinop University, Sinop, Turkey
[90]Also at Erciyes University, Kayseri, Turkey
[91]Also at Horia Hulubei National Institute of Physics and Nuclear Engineering (IFIN-HH), Bucharest, Romania
[92]Also at Texas A&M University at Qatar, Doha, Qatar
[93]Also at Kyungpook National University, Daegu, Korea
[94]Also at another institute or international laboratory covered by a cooperation agreement with CERN
[95]Also at Universiteit Antwerpen, Antwerpen, Belgium
[96]Also at Yerevan Physics Institute, Yerevan, Armenia
[97]Also at Northeastern University, Boston, Massachusetts, USA
[98]Also at Imperial College, London, United Kingdom
[99]Also at Institute of Nuclear Physics of the Uzbekistan Academy of Sciences, Tashkent, Uzbekistan